

AD-A169 718

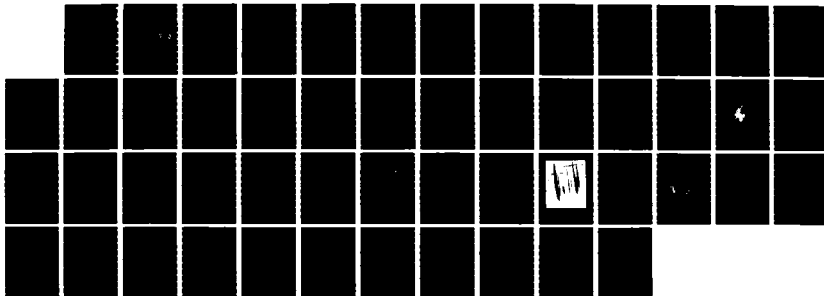
A STRIATION MODEL AND SPECTRAL CHARACTERISTICS OF
OPTICAL-IR EMISSION FROM (U) NAVAL RESEARCH LAB
WASHINGTON DC E HYMAN ET AL. 30 APR 85 NRL-MR-3568

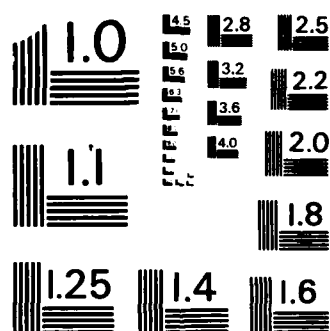
1/1

UNCLASSIFIED

F/G 18/3

NL





MICROCOPY RESOLUTION TEST CHART
NATIONAL BUREAU OF STANDARDS - 1963 - A

2

NRL Memorandum Report 5568

A Striation Model and Spectral Characteristics of Optical-IR Emission from HANE

E. HYMAN,* M. MULBRANDON AND N. J. ZABUSKY†

*Geophysical and Plasma Dynamics Branch
Plasma Physics Division*

**Science Applications International Corp.
McLean, VA 22102*

*†Fluid Sciences, Inc.
Pittsburgh, PA 15261*

AD-A169 718

April 30, 1985

DTIC
ELECTE
JUL 24 1986
S D

This research was sponsored by the Defense Nuclear Agency under Subtask S99QMSRI,
work unit 00018 and work unit title "Infrared Structure."



NAVAL RESEARCH LABORATORY
Washington, D.C.

Approved for public release; distribution unlimited

mic FILE COPY

00 5

AD - A169718

REPORT DOCUMENTATION PAGE				
1a REPORT SECURITY CLASSIFICATION UNCLASSIFIED		1b RESTRICTIVE MARKINGS		
2a SECURITY CLASSIFICATION AUTHORITY		3 DISTRIBUTION/AVAILABILITY OF REPORT		
2b DECLASSIFICATION/DOWNGRADING SCHEDULE		Approved for public release; distribution unlimited.		
4 PERFORMING ORGANIZATION REPORT NUMBER(S) NRL Memorandum Report 5568		5 MONITORING ORGANIZATION REPORT NUMBER(S)		
6a NAME OF PERFORMING ORGANIZATION Naval Research Laboratory	6b OFFICE SYMBOL (If applicable) Code 4780	7a NAME OF MONITORING ORGANIZATION		
6c ADDRESS (City, State, and ZIP Code) Washington, DC 20375-5000		7b ADDRESS (City, State, and ZIP Code)		
9a NAME OF FUNDING/SPONSORING ORGANIZATION Defense Nuclear Agency	8b OFFICE SYMBOL (If applicable) RAAE	9 PROCUREMENT INSTRUMENT IDENTIFICATION NUMBER		
9c ADDRESS (City, State, and ZIP Code) Washington, DC 20305		10 SOURCE OF FUNDING NUMBERS		
		PROGRAM ELEMENT NO 62715H	PROJECT NO	TASK NO DN080-323
11 TITLE (Include Security Classification) A Striation Model and Spectral Characteristics of Optical-IR Emission from HANE				
12 PERSONAL AUTHOR(S) Hyman, E.,* Mulbrandon, M. and Zabusky, N.J.†				
13a TYPE OF REPORT Interim	13b TIME COVERED FROM 10/84 TO 10/85	14 DATE OF REPORT (Year, Month, Day) 1985 April 30	15 PAGE COUNT 51	
16 SUPPLEMENTARY NOTATION *Science Applications International Corp., McLean, VA 22102 †Fluid Sciences, Inc., Pittsburgh, PA 15261 (Continues)				
17 COSATI CODES		18 SUBJECT TERMS (Continue on reverse if necessary and identify by block number)		
FIELD	GROUP	SUB-GROUP		
19 ABSTRACT (Continue on reverse if necessary and identify by block number)				
<p>An analytical model of a late-time high-altitude ionospheric striation is presented which incorporates characteristic shapes from recent NRL simulations. The model striation is nonaxisymmetric with a long diffuse tail (frontside), a compact core, and a steep backside. It contains six adjustable parameters to vary the shape and edge properties for sensitivity studies. We vary model parameters and investigate the power spectral density (PSD) as observed from different view angles. We compare results of the model with Chesnut's PSD obtained from photographs of Checkmate. A good fit is obtained with our model without any size distribution of striations.</p>				
20 DISTRIBUTION/AVAILABILITY OF ABSTRACT <input checked="" type="checkbox"/> UNCLASSIFIED UNLIMITED <input type="checkbox"/> SAME AS RPT <input type="checkbox"/> DTIC USERS		21 ABSTRACT SECURITY CLASSIFICATION UNCLASSIFIED		
22a NAME OF RESPONSIBLE INDIVIDUAL J. D. Huba		22b TELEPHONE (Include Area Code) (202) 767-3630		22c OFFICE SYMBOL Code 4780

16. SUPPLEMENTARY NOTATION (Continued)

This research was sponsored by the Defense Nuclear Agency under Subtask S99QMSRI, work unit 00018 and work unit title "Infrared Structure."

CONTENTS

1. INTRODUCTION	1
2. A STRIATION MODEL	3
3. SCANS	6
4. SPECTRAL PROPERTIES	8
5. COMPARISON WITH CHECKMATE DATA	15
6. SUMMARY	19
ACKNOWLEDGMENTS	20
REFERENCES	37

Accession For	
NTIS CRA&I	<input checked="" type="checkbox"/>
DTIC TAB	<input type="checkbox"/>
Unannounced	<input type="checkbox"/>
Justification	
By	
Distribution /	
Availability Codes	
Dist	Avail and/or Special
A-1	



A STRIATION MODEL AND SPECTRAL CHARACTERISTICS OF OPTICAL-IR EMISSION FROM HANE

I. INTRODUCTION

This is the third in a series of papers which use a deterministic approach to estimate spatial spectral indices of optical data from sensors which view structured plasma clouds in the high altitude disturbed atmosphere. In the first paper⁽¹⁾ we considered idealized functions of one variable which could represent scans. We established the relationship between continuity properties of these "profile" or "scan" functions, or their derivatives, and the spectral index of their Fourier transforms. We provided numerical examples using simple symmetric geometric figures to illustrate the errors that arise in estimating spectral indices. We estimated the minimum number of modes required to provide a specified accuracy in the asymptotic spectral index. For example to recover the -4 index of the power spectral density of a trapezoid (a profile with three possible space regions) requires about 10,000 modes.

In a second paper⁽²⁾ we related the asymptotic spectral index of a radiating cloud to that of a scan of the cloud. The theory is applicable to convex piecewise constant clouds

Manuscript approved March 5, 1985.

and to more realistic clouds which have polynomial flanks. We used the results of these papers to analyze optical scans from the PLACES experiment. We found that the data has insufficient resolution to determine an asymptotic spectral index associated with nonlinear dynamical (steepening) processes.

In this paper we describe an asymmetrical 6-parameter analytical model suggested by recent computer simulations to represent an isolated late-time high altitude striation from a high altitude nuclear event (HANE). Our early spectral studies⁽³⁾ made direct use of numerical simulation results of barium releases⁽⁴⁾. However, the inadequate resolution of sharp gradients and the uncertainties concerning the small-scale physical processes led us to develop an analytical model. The model is easy to use in a sensitivity study and is consistent with available HANE and barium cloud data.

In Section 2 we describe a striation model and in Section 3 we introduce scans. In Section 4 we discuss its spectral properties as we vary parameters of the model and as we change the direction of observation. In Section 5 we examine Checkmate optical data and analyze it in terms of our analytical model. In Section 6 we summarize the results of this paper.

2. A STRIATION MODEL

The growth of striations in the late-time high altitude ionosphere is believed to be mediated by a gradient drift instability. When there is relative motion between a plasma and the background gas in a direction perpendicular to the earth's magnetic field, a steepening of plasma density occurs on the backside of the cloud (that is, the side opposite the direction in which the cloud is moving). In the plane perpendicular to the magnetic field, the cloud becomes elongated in the direction along the relative velocity vectors and narrows somewhat in the transverse direction (see Figure 1). The instability induces the formation of striations at the backside which can lead to one or more bifurcations of the cloud.

Recent theoretical and numerical investigations of Zalesak, et al,^{(5),(6)} at NRL employ a new diffusivity model. They show that high conductivity clouds form a long lasting compact core even while the edges diffuse rapidly and, thus, bifurcations are suppressed and the result is a stable 'frozen' striation over extended times. In addition, new features are observed including a more extended diffuse frontside (tadpole tail) and a more rounded steep backside than with previous diffusivity models.

We cannot be certain that the striations that form in the nuclear environment will have the above characteristic shape. The simulations performed for the barium case are a result of the specific ionospheric parameters in that situation. In the nuclear case cloud conductivity is typically much higher, for example. Also, the ratio of plasma to neutral density could be much different. Until simulations with parameters more relevant to specific nuclear events are performed the validity of the model we are proposing will be open to question. Nevertheless, we believe it is instructive to study the properties of a non-axisymmetric striation to identify the observational consequences.

We have constructed a simple 6 parameter analytical model which incorporates these essential new properties. Figure 2 illustrates the model in a plane perpendicular to the magnetic field. Although our model is two dimensional, one could easily introduce a gradual Gaussian dependence along the magnetic field with a scale length large compared to dimensions in the plane.⁽³⁾ Transverse to the field the equation representing the model is

$$\begin{aligned}
 F(r, \theta) &= F_{\text{MAX}} (1. - \exp(-A)); & r &\leq R_1(\theta) \\
 &= F_{\text{MAX}} \left[\exp \left[-A \left(\frac{r - R_1(\theta)}{R_2(\theta) - R_1(\theta)} \right)^2 \right] - \exp(-A) \right]; & R_1(\theta) < r < R_2(\theta) \\
 &= 0.0 & ; & \quad r \geq R_2(\theta) \quad (1)
 \end{aligned}$$

where

$$R_i(\theta) = \rho_{Bi}\rho_{Ci}/[\rho_{Bi}^2\cos^2\theta + \rho_{Ci}^2\sin^2\theta]^{\frac{1}{2}}, \quad -\frac{\pi}{2} < \theta < \frac{\pi}{2}$$

$$R_i(\theta) = \rho_{Fi}\rho_{Ci}/[\rho_{Fi}^2\cos^2\theta + \rho_{Ci}^2\sin^2\theta]^{\frac{1}{2}}, \quad \frac{\pi}{2} < \theta < \frac{3\pi}{2}$$

where θ is measured from the backside direction and $i = 1$ or 2 . Here $R_1(\theta)$ bounds the constant density core and $R_2(\theta)$ bounds the cloud. These boundaries are each parameterized by three constants: ρ_{Bi} and ρ_{Fi} are semiaxes of the ellipses in the backside and frontside directions, respectively, and ρ_{Ci} are the common semiaxes at $\theta = \pm \pi/2$. Where the two ellipses meet, their slopes, are identical. Between $R_1(\theta)$ and $R_2(\theta)$ the density falls off radially with a Gaussian dependence which is a function of angle and vanishes at $R_2(\theta)$. Note the slope of F is discontinuous at $R_2(\theta)$.

In the discussions below and in Section 3 we have chosen the following values to define the striation: tail length $\rho_{F2} = 5.0$ km, transverse core radius $\rho_{C1} = 0.5$ km, longitudinal core radii $\rho_{B1} = 0.6$ km and $\rho_{F1} = 0.3$ km. The edge sides $\rho_{B2}-\rho_{B1}$ and $\rho_{C2}-\rho_{C1}$ are varied for the different cases discussed. The parameter A was set equal to 3.

The spectral properties we will discuss are weakly dependent on the specific functional form chosen but are sensitive to the non-axisymmetric properties. The

particular functional form for the striation model given by Equation (1) has no fundamental significance.

We use it because with as few as 6 parameters it correctly reproduces the known properties of striations established in current simulation studies.

3. SCANS

Suppose we imagine a detector sufficiently distant from the striation that the rays emitted from the cloud can be assumed to be parallel. We will assume that the radiation is optically thin so that we just add the contributions of the emission from all points in the striation along a line perpendicular to the scan. We can scan across the striation from a variety of observational locations. If we define the observation angle as the angle the detector makes with the long axis of the striation, then a scan in the direction from the backside edge through the tail is 0° (Figure 2).

To perform numerically a scan on the model striation and obtain the profile from a given observational direction a rectangular 256×256 grid is imposed. In Figure 2, imagine a grid coordinate system parallel and perpendicular to the long axis of the striation. For example, to do a 0° scan, the vertical spacing will be much smaller than the horizontal spacing so as to just enclose the striation, with little grid spacing outside. To do a 45° scan the striation is rotated (not the grid) so that interpolation to the grid

points is never necessary. To obtain a maximum resolution and assure that the grid just encloses the striation, only the grid spacings are changed as we change scan angle. We then simply sum grid values along an observational direction for each perpendicular grid point.

A scan at 0° results in a symmetric radiance profile, Figure 3, in which we have assumed that the radiative emission from each point of the striation is proportional to the electron density at that point. The units for the ordinate are arbitrary. The abscissa is in km. The ellipse parameters for this profile were chosen so that back and side Gaussian edges are 0.1 km.

If we scan from a location transverse, 90° , (see Figure 2) the resulting radiance profile, given in Figure 4, is highly skewed with the steep region corresponding to the steep gradients at the backside edge. The other side of this profile has a very gradual falloff due to the long diffuse tail. Note, that Figure 4 has a different abscissa scale than in Figure 3. In general, we wish to investigate the spectral properties of this model as a function of viewing angle, as we vary the size of the edges. This will be described in the following section.

4. SPECTRAL PROPERTIES

As we have shown in reference 1, the spectral properties of the profile of an optical scan (for example, the spectral index of the asymptotic envelope) are influenced by the nature of the discontinuities in the profile function or its derivatives. The scale size of any characteristic segment of the profile is manifest in a corresponding region of the power spectral density (PSD) in an inverse sense, i.e. large sizes affect low mode numbers and small sizes affect high mode number regions of the PSD. Within each scale-size regime the most severe discontinuities lead to the slowest falloff with mode number and, hence, dominate the PSD if they represent a source strength comparable to other portions of the profile. In the following paragraphs we present typical PSD's obtained from our model showing the effect of angle variation with thin edges and with thicker edges and we show the differences obtained when the emission is proportional to the square of the electron density.

4.1 Thin Edge Results

Figure 5 is a log-log plot of the PSD for scans of the model of Figure 2 at 0° (unconnected dots) and at 90° (solid line), in which we have taken the back and side edges to be 0.05 km. We have drawn in k^{-3} and k^{-4} lines to facilitate

analysis. The ordinate is normalized so that the area under the curve is unity. There are two scales on the abscissa. The lower scale is the wavelength ($2\pi/k$) in km, where $k = \pi\nu/L$, ν is the mode number, and the region ranges from $-L$ to L . (As stated previously, the scan consists of 256 non-zero values, and these are on a grid of 4096 points.) The upper scale gives the mode number, ν , which ranges from 1 to 2048. The mode number in this figure is appropriate only for the 0° case which is for a scan over 1 km (whereas the 90° view consists of a scan over ~ 6 km, and they both have the same number of grid points). Note, also the well defined maxima and minima in the 0° PSD, characteristic of a symmetric profile such as Figure 3 and absent in the 90° case.

The 90° PSD has a spectral index ≈ -3 . To understand this consider the profile of Figure 4. On a scale size ≈ 1 km the profile consists of two segments: first, the profile of the constant density, elliptically bounded core region and second, the profile of the tail region. The contribution of the first segment to the PSD falls off like k^{-3} , where k is proportional to the mode number,⁽¹⁾ and that of the second segment has a Gaussian falloff (the PSD of a Gaussian is a Gaussian). Since the radiative emission from the tail is comparable to that from the core region and the power in this region falls off much faster with k , the spectral character will be dominated by that of the core

region and there will be a k^{-3} falloff in the PSD. If we consider scale sizes 0.1 km we need to focus on the profile of the backside edge, which is Gaussian. Since this is the only profile segment on this scale size or smaller, the PSD will change from a k^{-3} to a Gaussian falloff at sufficiently large mode number. Because of insufficient resolution, the 90° curve never exhibits the anticipated large- k Gaussian falloff.

For the 0° scan there appears to be an intermediate region with a k^{-3} envelope that matches the 90° PSD. This is a reflection of the constant density, elliptically bounded core region, as in the 90° profile. At higher k , corresponding to scale sizes $\lesssim 0.1$ km, the PSD is determined by the steep flank edges of the striation. Here we have sufficient resolution to see the Gaussian falloff at these k values.

Note the profile of Figure 3 can be approximately fit alternatively with a single semicircle of radius 0.5 km or a trapezoid of parallel sides 0.2 and 1.06 km, respectively. The former gives a k^{-3} PSD in agreement with Figure 5 whereas the latter, in which the scales are not well-separated, gives a k^{-4} PSD. However, the latter gives nulls at 0.62 km, 0.43 km, 0.315 km, etc. in agreement with Figure 3 whereas the nulls of the former are not in good

agreement with Figure 3. Furthermore, the PSD obtained from the trapezoidal fit to Figure 3 is a very good fit to the model PSD up to the third minimum. This shows the difficulty of assessing a PSD from qualitative considerations.

4.2 Thicker Edge Results

The example we have just used has one simplifying property, that we chose an edge size small compared to the core region. This provided a good separation of scales between the Gaussian edge region and the core region. Let us consider another example in which now the backside edge is 0.1 km and the flanks are 0.3 km. This is a realistic case, since simulations show that flanks have thicker edges than backsides.

To have a well-defined falloff before the Gaussian edge intrudes, the effective width of the profile must be substantially larger than the edge size. Now, if we scan from 0° the profile size is ~1. km and the Gaussian edge is 0.3 km which provides insufficient range in k space. Thus, we would expect the Gaussian falloff to intrude well into even the low modes of the spectrum and that there will not be any clearly defined k^{-4} or k^{-3} region. On the other hand, at 90° the effective profile size is > 1 km which

compares with an edge size of 0.1 km so that there is a reasonable separation of scales. We expect a well-defined k^{-3} region.

Figure 6 shows the PSD of this model, observed from an angle of 10° . The line drawn in is k^{-3} and clearly shows there is no k^{-3} (nor is there a k^{-4}) region. Figure 7 shows the PSD as viewed from an angle of 80° . Again, the k^{-3} line is drawn in and shows a good fit down to ~ 0.2 km, where the Gaussian falloff begins to dominate. In TABLE I we show the "apparent" spectral index for this model as a function of angle. (The apparent index was obtained by a least squares fit to the data for angles $\geq 40^\circ$ from the first maximum to the wavelength of Gaussian onset (last column). At smaller angles this breaks down and the index is estimated.) At angles less than $\sim 40^\circ$ there is no k^{-3} region at all.

4.3 Emission Proportional to the Square of the Electron Density

Consider, now, a striation with Gaussian edges of 0.1 km. We want to compare the profile for this striation at 0° with a striation of the same size and shape but in which the radiative emission is proportional to the square of the electron density (N^2) rather than proportional to the electron density (N) itself. This is what will be observed if the striations consist of a recombining plasma rather

than debris ions being excited by solar uv or earthshine ir. Figure 8 shows the 'squared' profile which can be compared with the 'unsquared' one, Figure 3. What we see is a considerably more peaked profile, more triangular in shape, and, therefore, even more likely to exhibit a spectrum with a substantial k^{-4} region.

Figures 9 and 10 are the spectra for N and N^2 profiles respectively. Both have an overall k^{-4} falloff. In the N^2 case the Gaussian falloff is not manifest at as low k-values as in the N case. This follows because the Gaussian 'width' in the squared case has been reduced by \sqrt{I} and, therefore, constitutes a smaller perturbation on the rest of the profile.

TABLE 1
ANGULAR VARIATION IN CLOUD MODEL
(EDGES VARYING BETWEEN 0.1 and 0.3 KM)

<u>Angle</u>	<u>Spectral Index</u> <u>From Least Squares Fit</u>	<u>Wavelength of</u> <u>Gaussian Onset</u>
0°	-6.	-
10°	-6.	-
20°	4.3	-
30°	3.6	-
40°	3.5	0.45 km
50°	3.4	0.35 km
60°	3.5	0.31 km
70°	3.3	0.26 km
80°	3.2	0.26 km
90°	3.2	0.23 km

5. COMPARISON WITH CHECKMATE DATA

The Checkmate burst occurred at a high altitude south of Johnston Island (JI). The debris rose and became aligned with the earth's magnetic field and striations were observed. Figure 11 shows the approximate geometrical set up. The plane of the figure is along a north-south geomagnetic longitude determined by the vector from JI to the burst point and the camera axis. Photographs were taken by Chesnut looking north at ~ 300 sec and at other times. At 300 sec the camera elevation angle was such that the center of the photograph was approximately perpendicular to the magnetic field. The component of the ion-neutral relative velocity perpendicular to the field is, thus, aligned with the camera axis and our observation corresponds to a zero angle view (as defined in Figure 2). However, the photograph in Figure 12⁽⁷⁾ has an angular extent $\sim 30^\circ$, and thus striations are observed at various angles. The striations at the extremities may be more than 15° off axis if one accounts for debris motion out of the plane.

In the photograph of Figure 12 we see striations clumped into two major groups associated with our view through the arms of the Checkmate "horseshoe". Figure 13 is the PSD, obtained by Chesnut from scan 2 in Figure 12,

and plotted on a semi-log scale. The PSD has been smoothed by performing an average for each data point of the 31 adjacent data points. Chesnut has shown that if one assumes striations with axial symmetry, e.g. lucite rods or Gaussian rods, it is necessary to assume a range of sizes to adequately fit the data. In the case of Gaussians, for example, it was necessary to include striation sizes ranging from -2 km down to -0.29 km to fit the data. We will show that by using a nonaxially symmetric model of a striation with parameter ratios suggested by numerical simulations it is possible to fit the data well without resorting to a size distribution.

First, we need to establish the shape parameters of our model striation from Checkmate data. We assume that the single striation discussed by Chesnut⁽⁷⁾ is obtained from one of our striations observed at 10° with an aspect ratio (ρ_{F2}/ρ_{C1}) = 10. The mean width of 1.4 km given by Chesnut leads us to choose ρ_{F2} = 7 km, ρ_{C1} = 0.7 km, ρ_{B1} = 0.7 km, ρ_{F1} = 0.42 km, and edge sizes = 0.1 km. (Edge sizes, in fact, influence higher k values than the Checkmate data can resolve and, thus, are unimportant.)

Next we place 100 of these identical striations at random in two groups associated with the horseshoe. The range covered is 150 km to match roughly the linear extent

in the photographic scan. The groups have a mean separation of 80 km and the left and right groups have half widths of 15 km and 30 km respectively. The random selection is from a normal distribution. To simulate the diverse view angles in the photograph, we rotate striations in various regions along the scan. The resulting profile is shown in Figure 14. Note in obtaining a scan, the minimum transverse dimension of a striation has been sampled by at least 35 points.

To simulate the PSD obtained by Chesnut, Figure 13, we average 8 nearest-neighbor k-space data points of the square of the transform. (This corresponds closely to Chesnut's k space averaging.) The PSD obtained from this is plotted in Figure 15. We have plotted the Chesnut data of Figure 13 on this plot for comparison and indicated the film grain noise level and the fit region on the plot. The region at smaller k than the fit region represents the low level unstructured background which we have not modeled. The exact position of peaks in the Chesnut data is related to the exact placement of striations which we did not attempt to match.

It is clear that in the very limited fit region there is a good match between our model striation PSD and the data. Of course, this shows only that if the data has insufficient spectral range there are at least two distinct

models that can fit it equally well. There are likely to be other combinations of striation parameters that could give equally good fits. In Figure 16 we plot the PSD of Figure 15 on a more standard log-log scale. We plot the k^{-4} line and indicate the fit region on this plot.

The essential conclusions are: (1) if we accept the results of recent computer simulations and infer from them the approximate shape and dimensions of high-altitude striations we can, at least, match the PSD's obtained from the measured Checkmate data. (2) The region of k -space accessible with the Checkmate data is too small to definitively establish what is the correct model.

6. SUMMARY

There is good reason to believe that substantial regions of the ionosphere following HANE events will be characterized by a highly structured plasma and that the structuring will persist for hours. Since defense detectors typically operate in the ir and are sensitive to the nature of the structuring it is important to be able to predict the spatial characteristics of ir emissions. In this paper we have presented a simple analytical model which embodies present knowledge of late-time high altitude striations, based on theory and the simulations being performed at NRL. Those properties still uncertain have been parameterized. Using this model we are able to predict the PSD characteristics that result from striations as a function of shape parameters, edge sizes, and the angle of observation. These results are preliminary. First, there is still imperfect knowledge of some aspects of the physics incorporated in the simulations. Second, simulations to date have been more appropriate to the barium release scenario and need to be repeated for parameters more relevant to the HANE case. Finally, HANE data in the ir is essentially non-existent and available visible data (photographic) has insufficient range to distinguish among alternative models.

We are able to show that available Checkmate data can be fit as well by our nonaxisymmetric striation model, without incorporating a distribution of striation sizes, as it has been by an axially symmetric model with a range of striation sizes. Although the data has insufficient range to distinguish between these models, there is every reason to believe that striations are not axially symmetric and to expect PSD's to be affected substantially by the relative location of detector and striations. We believe it is important that further simulations be performed, more directly relevant to specific HANE events, to determine with greater confidence the essential properties of ionospheric plasma striations. As more sensitive and higher resolution detectors are developed it will become possible and necessary to distinguish among alternative striation models.

ACKNOWLEDGMENTS

We thank J. Fedder of NRL and W. Chesnut of SRI for many helpful discussions. This work was supported by the Defense Nuclear Agency.

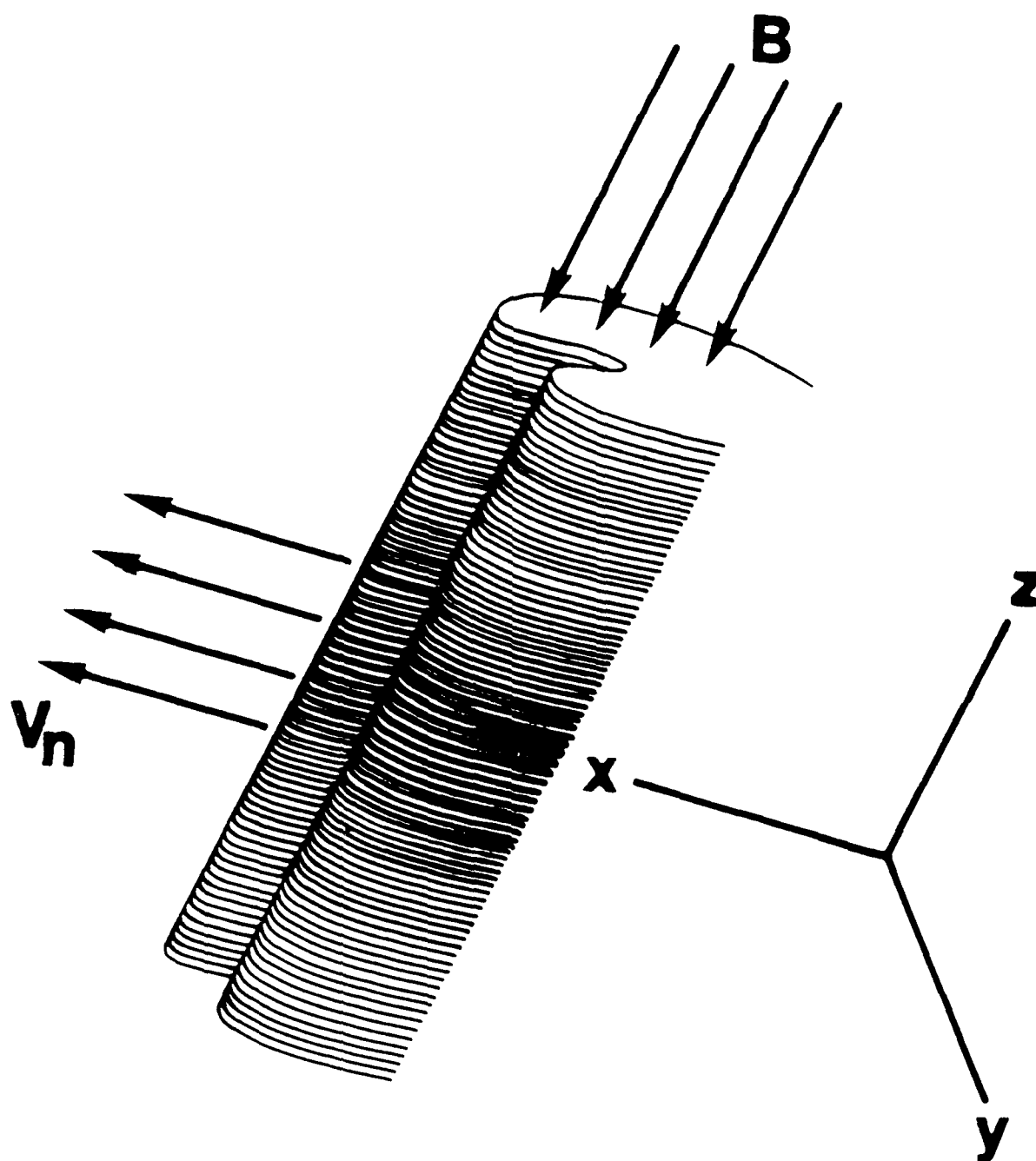


Figure 1 - Schematic view of ionospheric striation showing 'finger like' protuberances forming on the backside. The magnetic field direction, B , and neutral wind direction, V_n , are shown.

ANALYTIC MODEL FOR HANE STRIATION

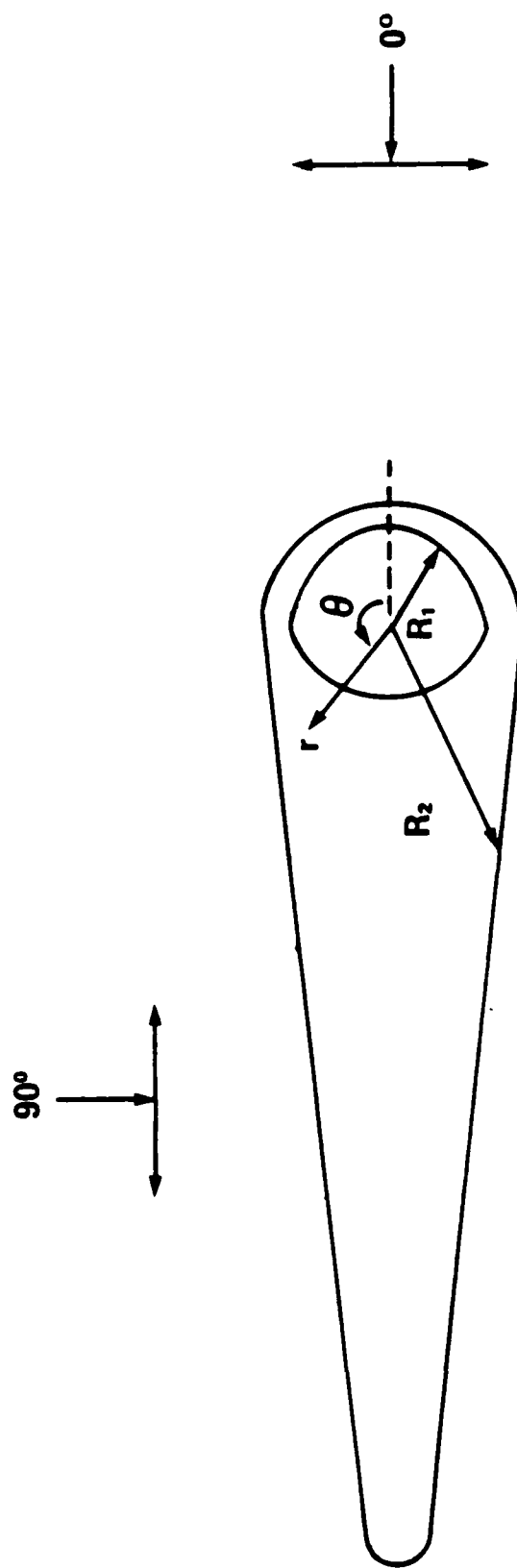


Figure 2 - Model striation in plane perpendicular to the magnetic field. $R_1(\theta)$ and $R_2(\theta)$ are given in Equation (1) of text. Scan directions of 0° and 90° are illustrated.

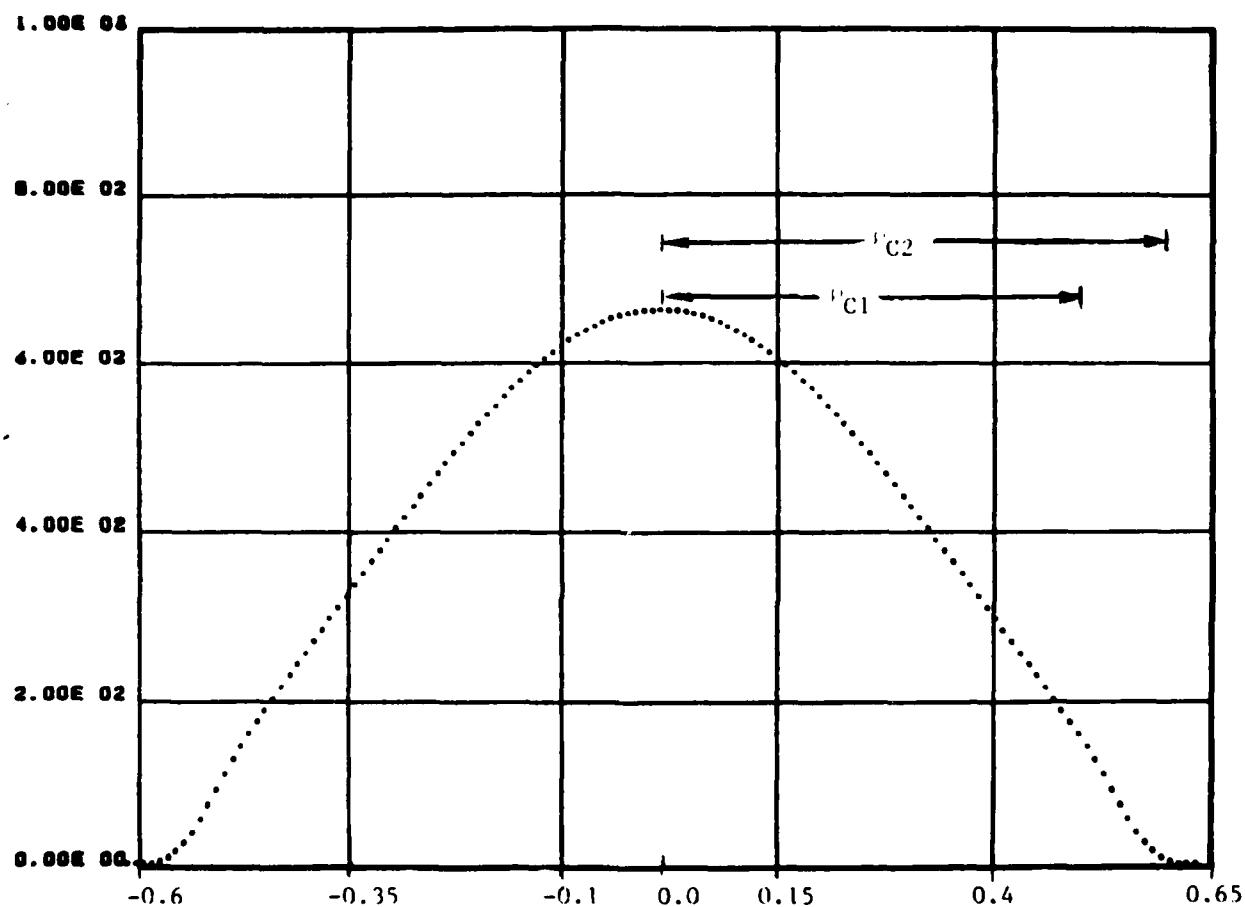


Figure 3 - Profile obtained from 0° scan of Figure 2. $\rho_{P1} = 0.3$ km, $\rho_{P2} = 5.0$ km, $\rho_{B1} = 0.6$ km, $\rho_{B2} = 0.7$ km, $\rho_{C1} = 0.5$ km, and $\rho_{C2} = 0.6$ km. The abscissa is in km and the ordinate is in arbitrary units.

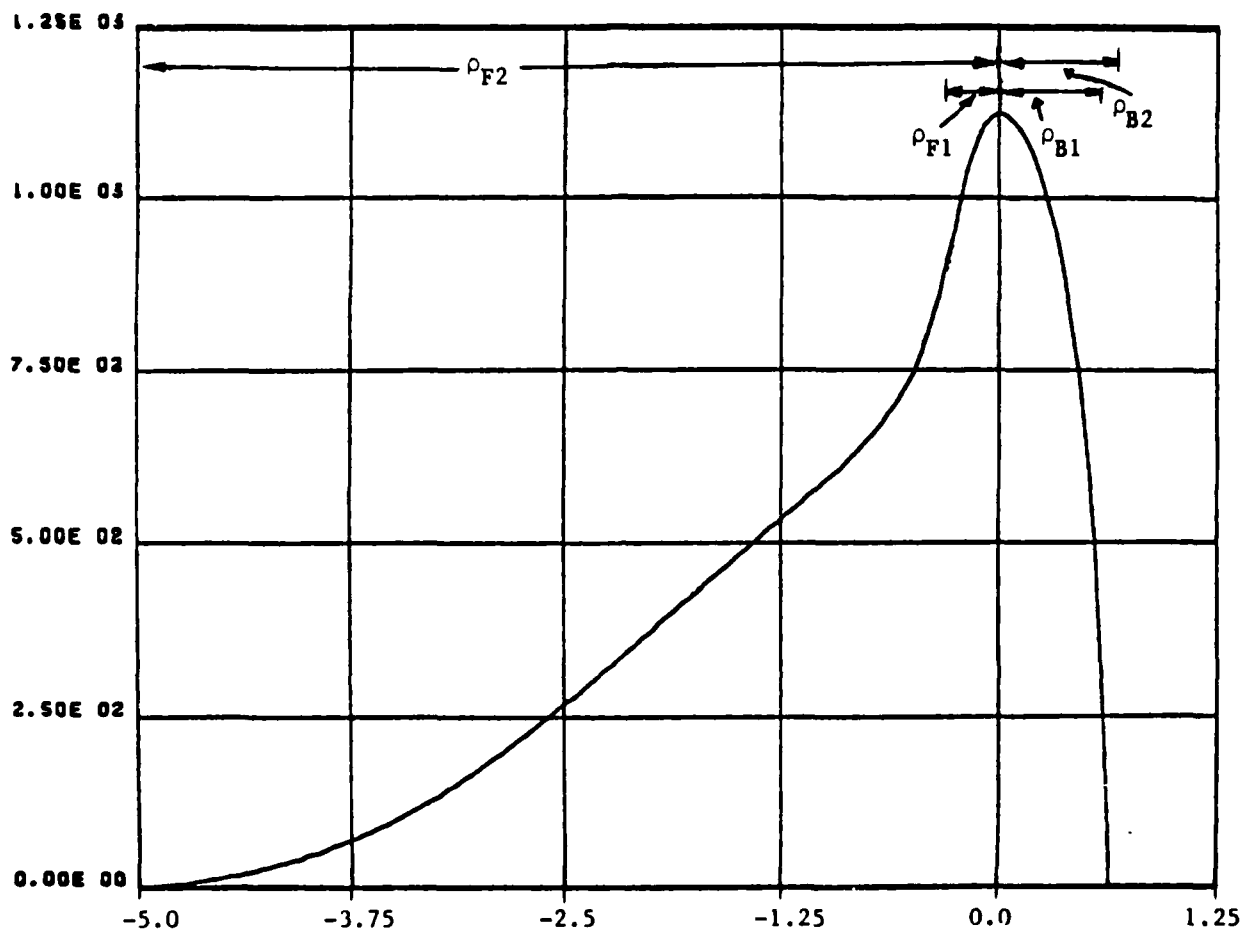


Figure 4 - Profile obtained from 90° scan of Figure 2. Same parameters as in Figure 3. Note the abscissa scale is 5 times that in Figure 3. The ordinate is in arbitrary units.

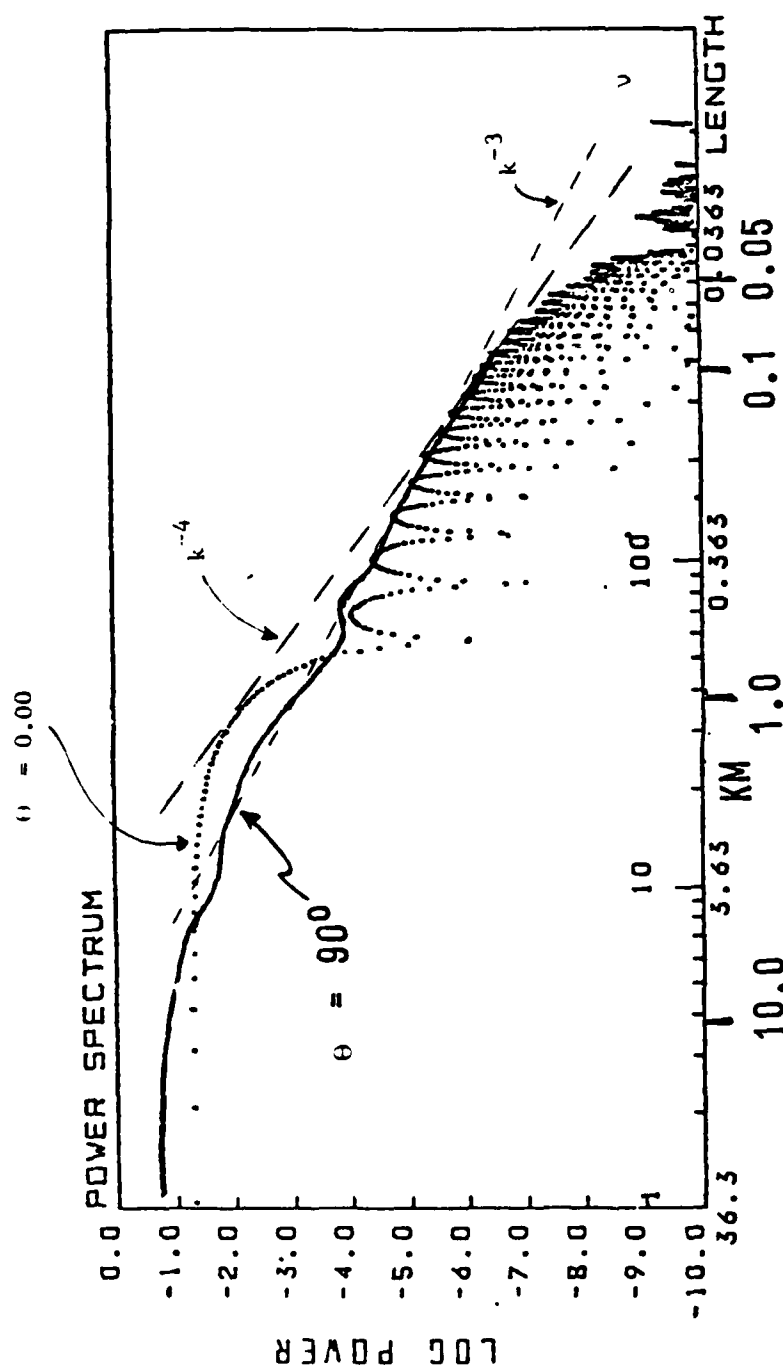


Figure 5 - PSD of 0° profile (unconnected dots) and 90° profile (solid line), with k^{-3} and k^{-4} lines added. Parameters are the same as in Figure 3 except $\rho B2 = 0.65\text{km}$ and $\rho C2 = 0.55\text{km}$. Ordinate is normalized to give unit area. Lower abscissa scale is spatial wavelength. Upper abscissa scale is mode number (applies to 0° case only).

$\theta = 10.00$

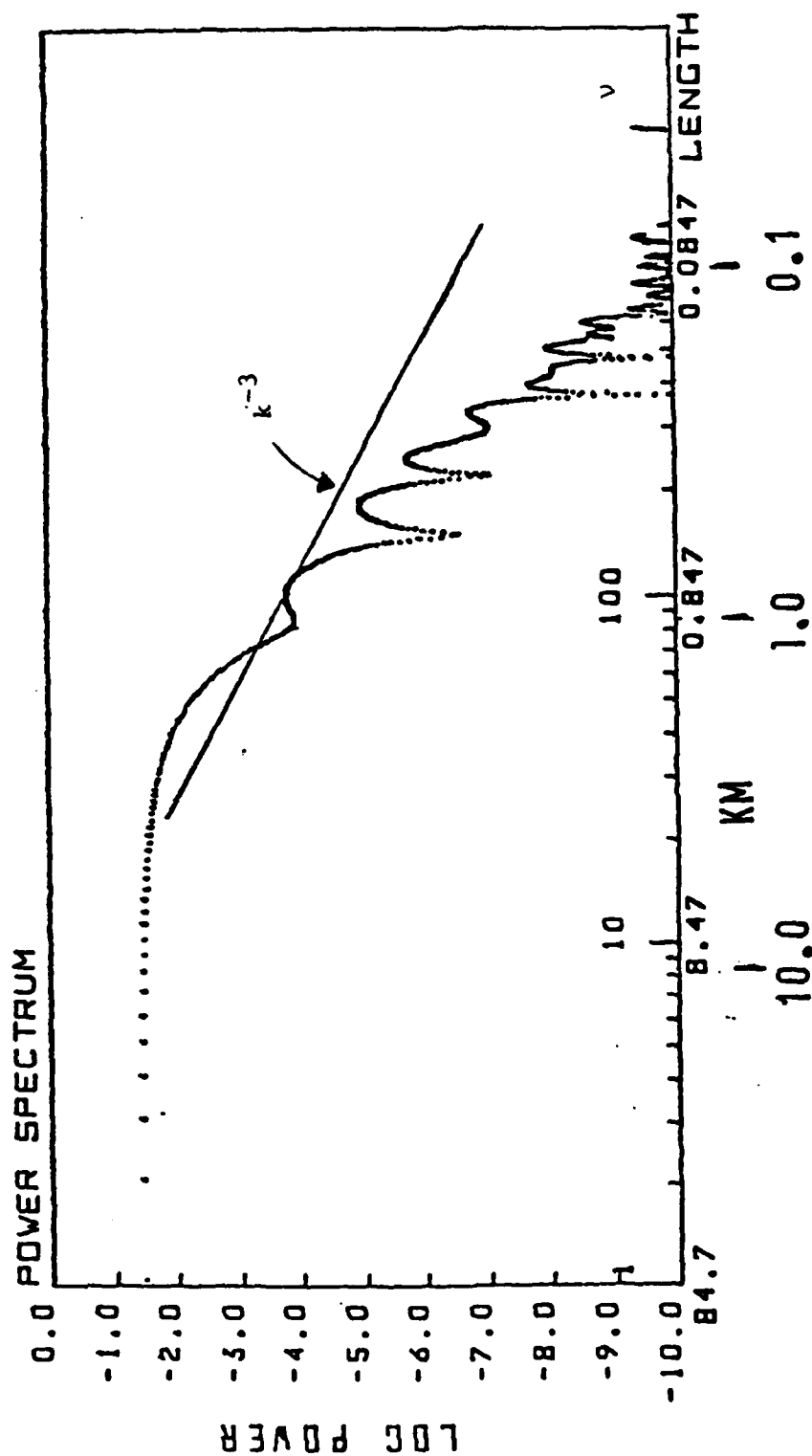


Figure 6 - PSD of 10° profile with k^{-3} line added. The parameters are the same as in Figure 3 except $\rho C_2 = 0.8\text{km}$. Scales are defined as in Figure 5.

$\theta = 80.00$

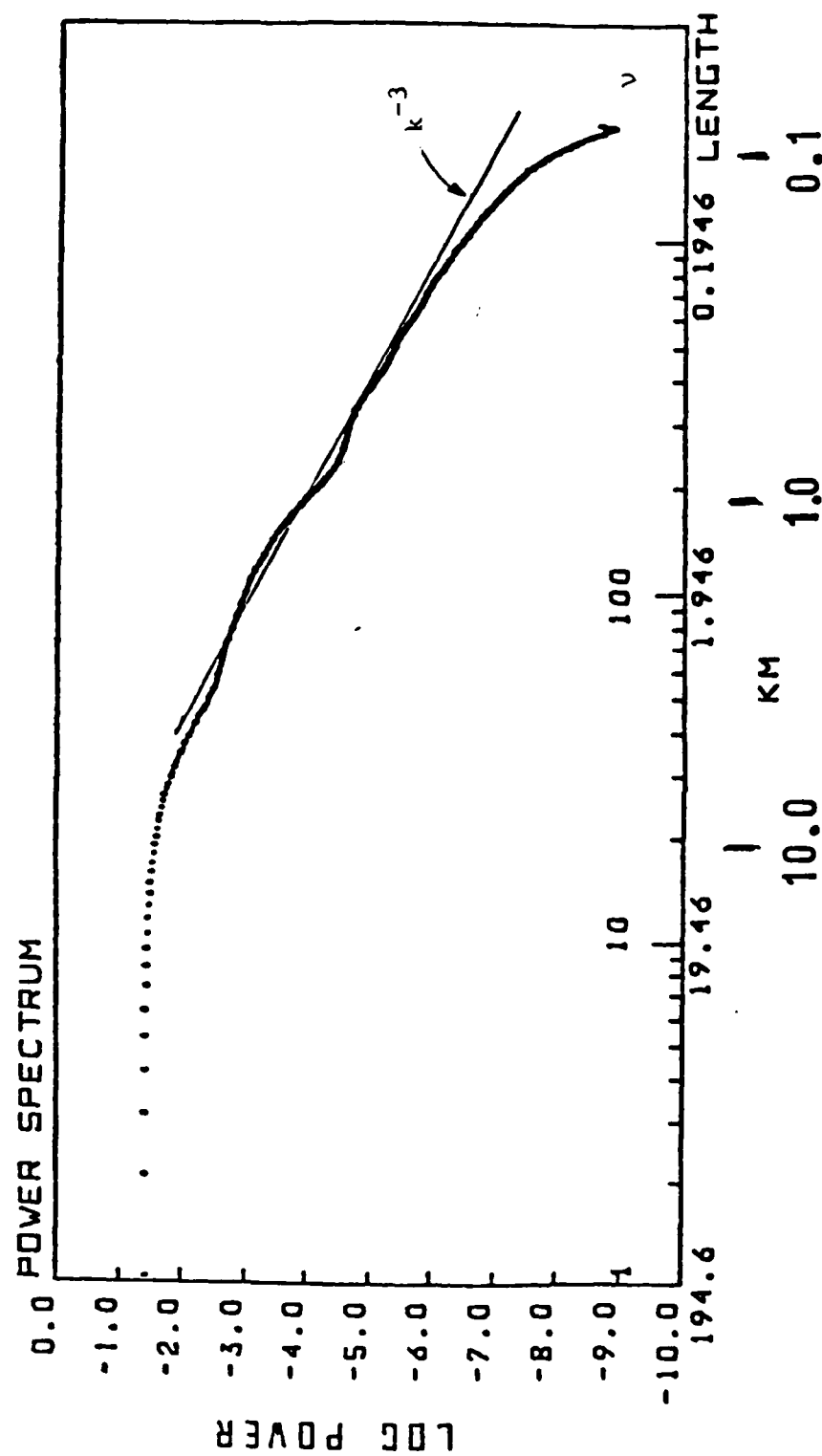


Figure 7 - PSD of 80° profile with k^{-3} line added. The parameters are the same as in Figure 6 and scales are defined in Figure 5.

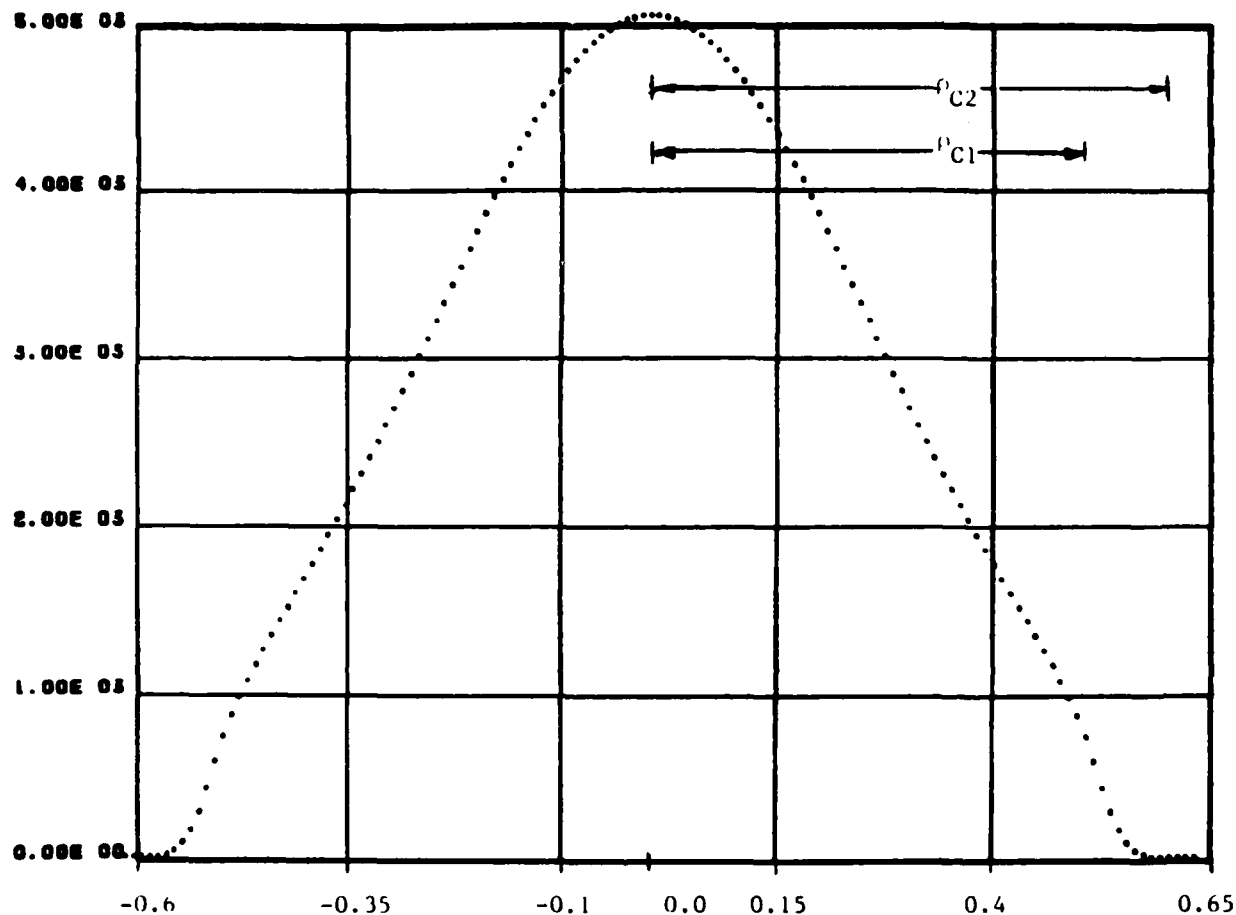


Figure 8 - Profile from 0° scan with parameters as in Figure 3, but radiative emission is assumed proportional to the square of the electron density (N^2). The abscissa is in km and the ordinate is arbitrary.

$\theta = 0.00$

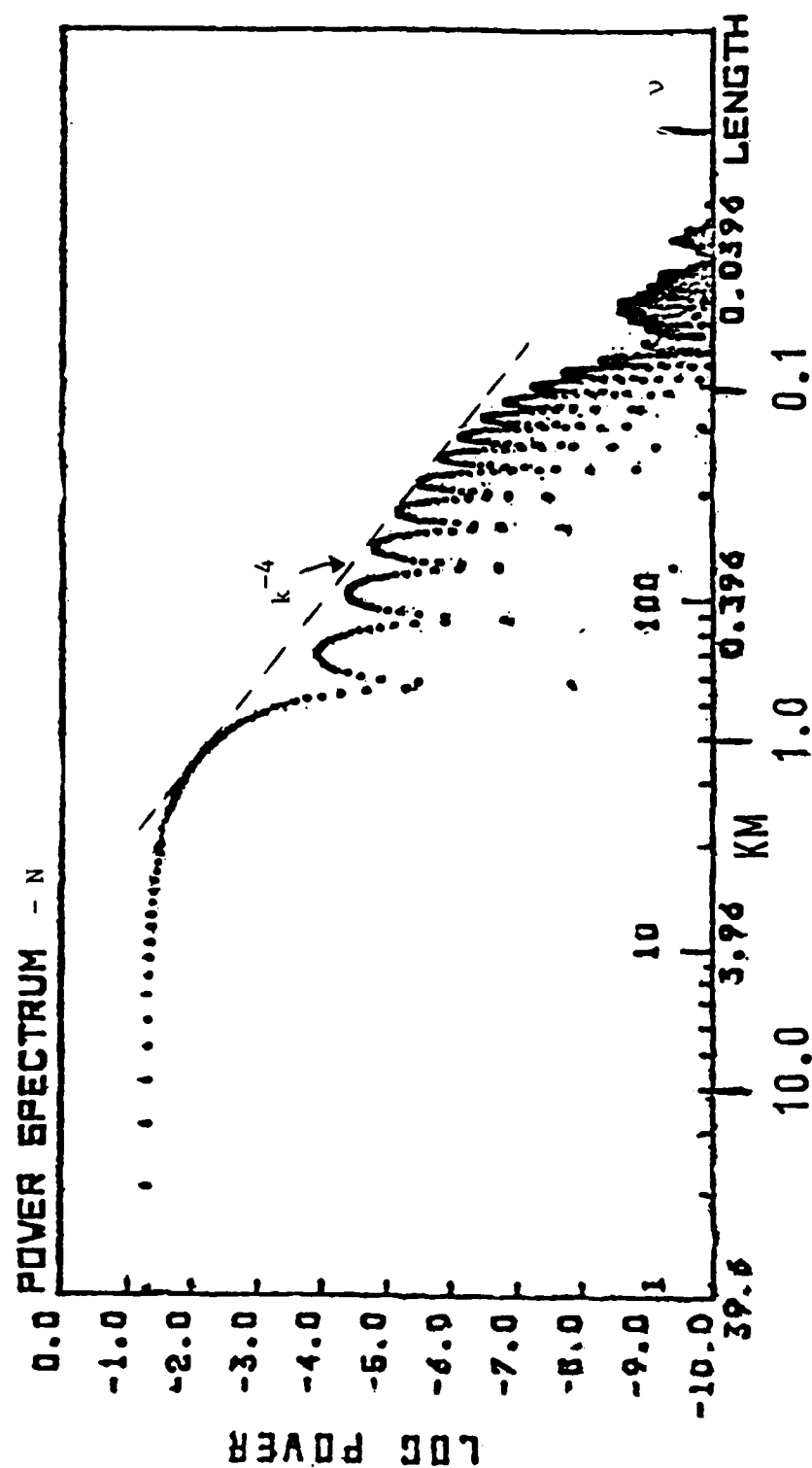


Figure 9 - PSD of 0° profile with parameters of Figure 3.

Scales as defined in Figure 5.

$$\theta = 0.00$$

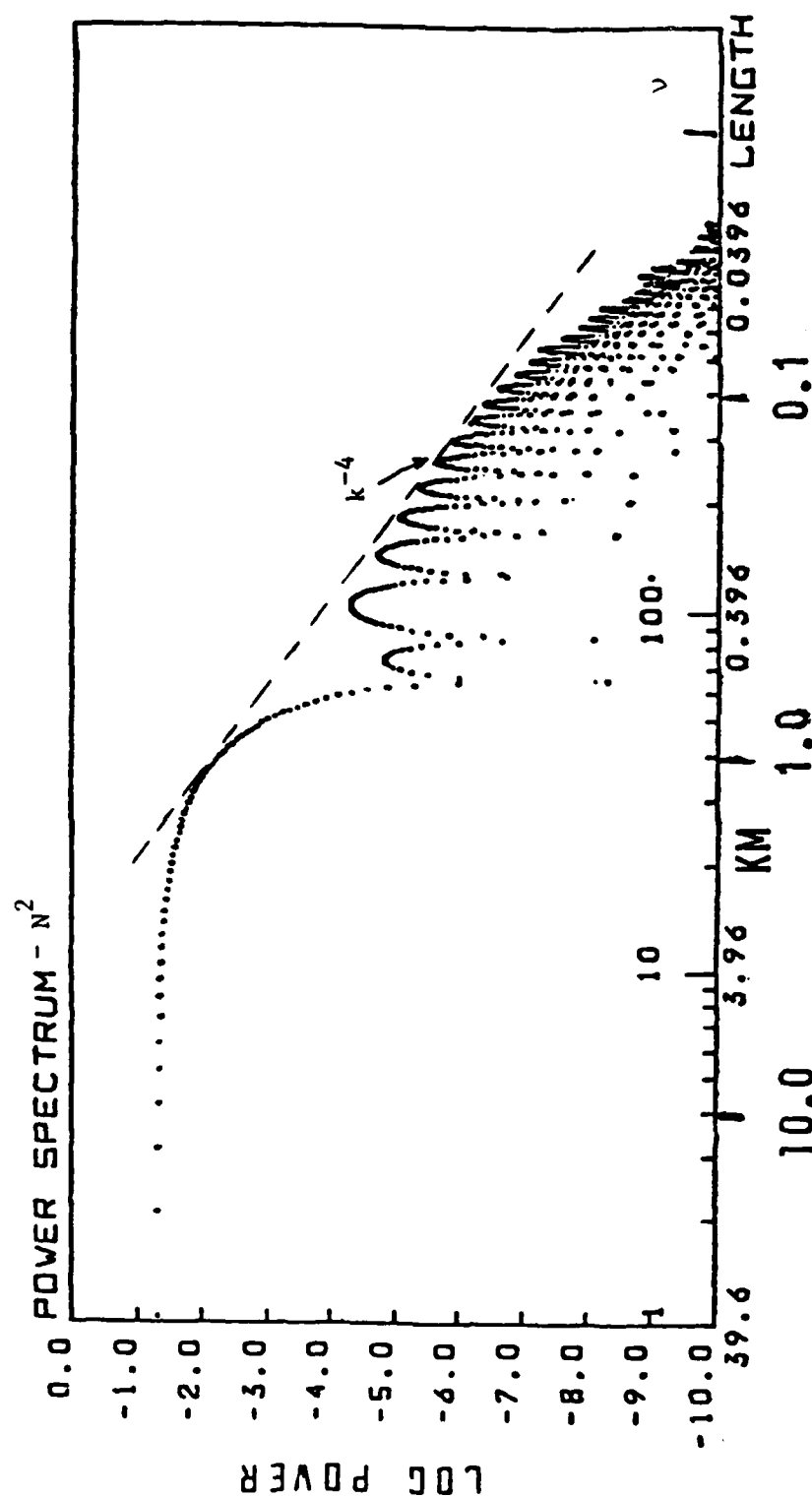


Figure 10- PSD of 0° profile of Figure 8. Parameters are the same as in Figure 3. Scales as defined in Figure 5.

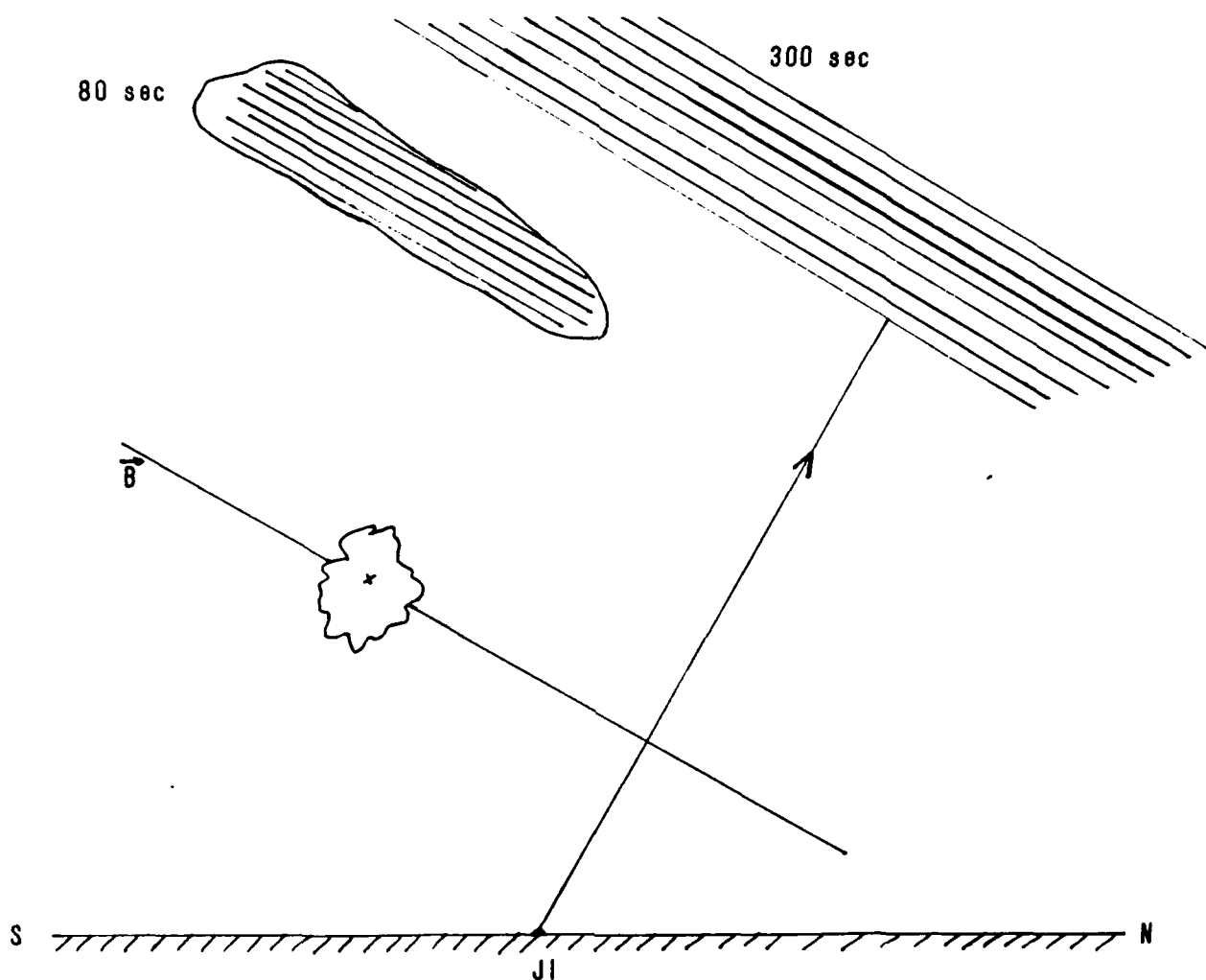


Figure 11- Schematic of Checkmate burst point and striations. Plane is north-south geomagnetic longitude including camera position at Johnston Island (JI), burst point, and camera axis. B is the ambient magnetic field direction.

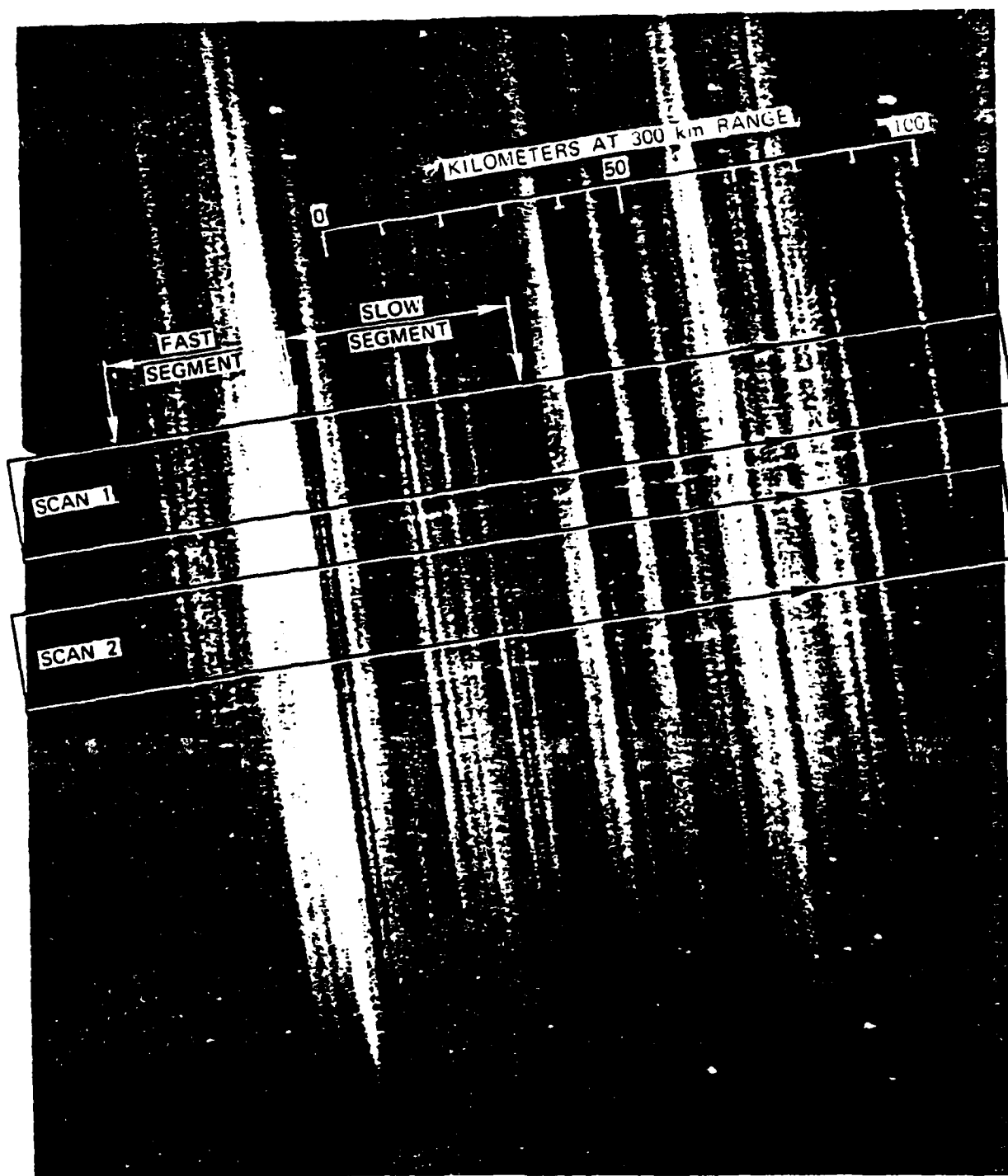


Figure 12- Photograph of Checkmate striations at 300 sec.
(Reference 7, Figure 2). Various scans are
illustrated.

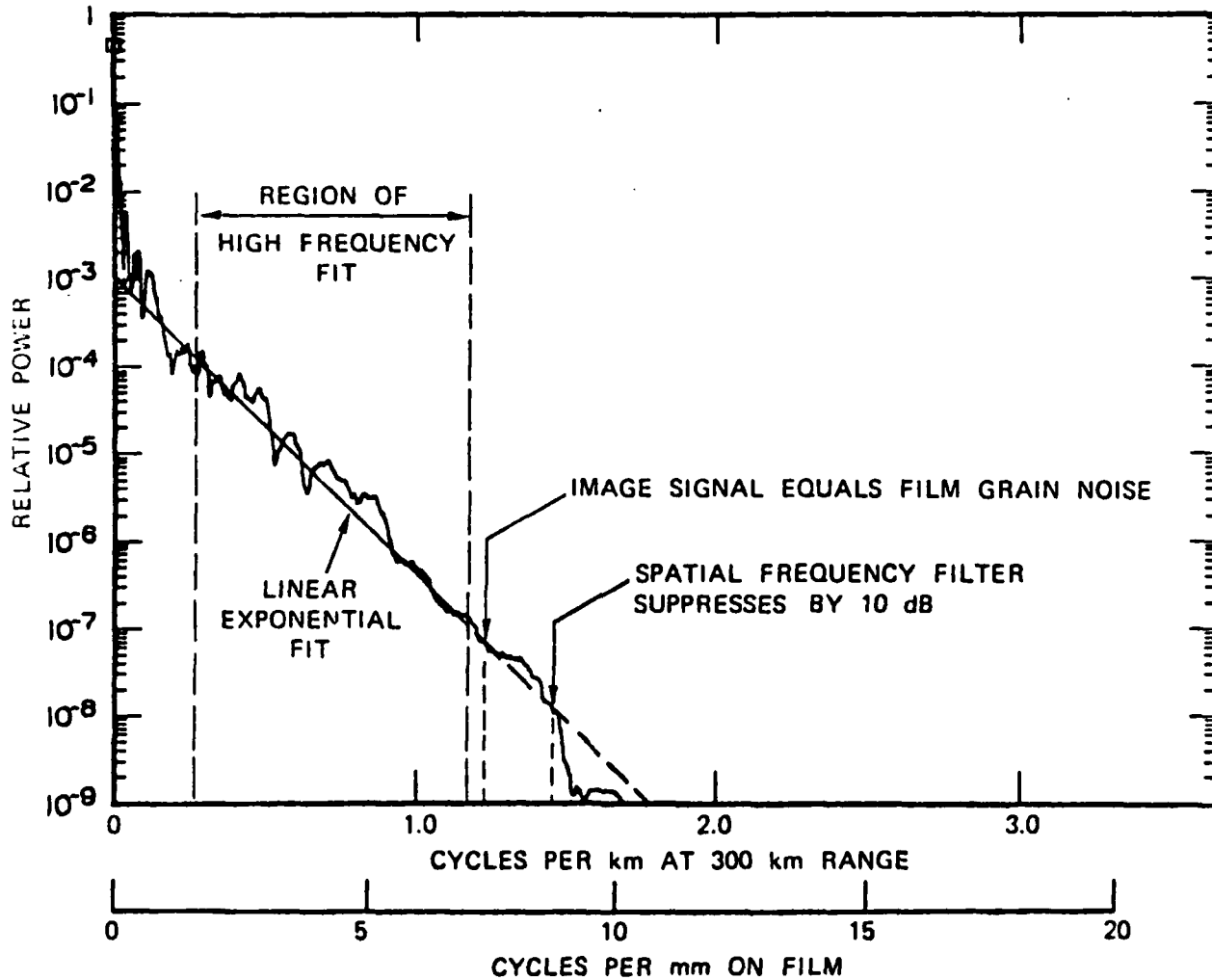


Figure 13- PSD of Scan 2 of Figure 12 (Reference 7, Figure 10) of Checkmate striations, plotted semi-log.

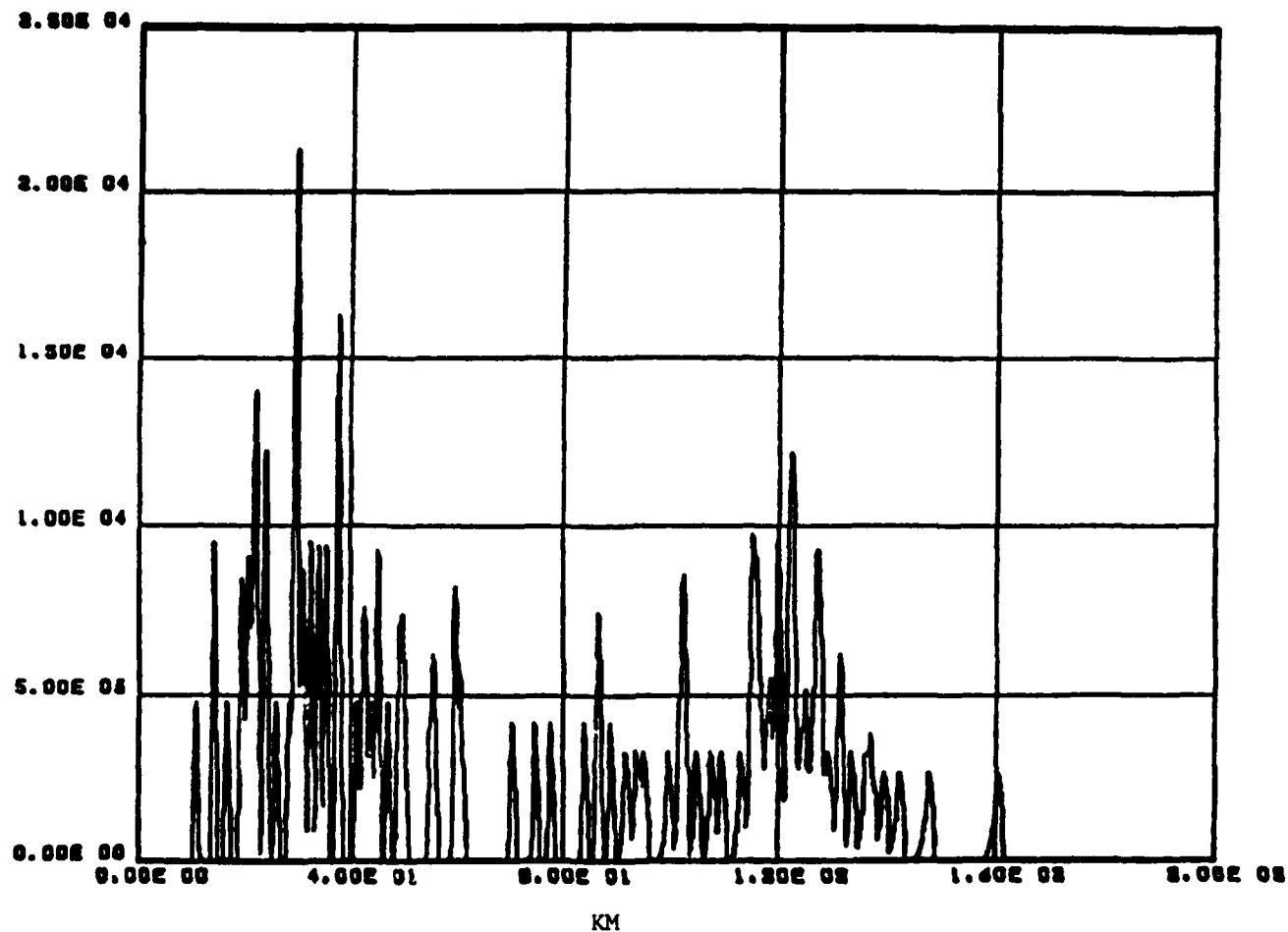


Figure 14- The profile of 100 striations placed to simulate a Checkmate scan. See text for details. The abscissa is in km and the ordinate is arbitrary.

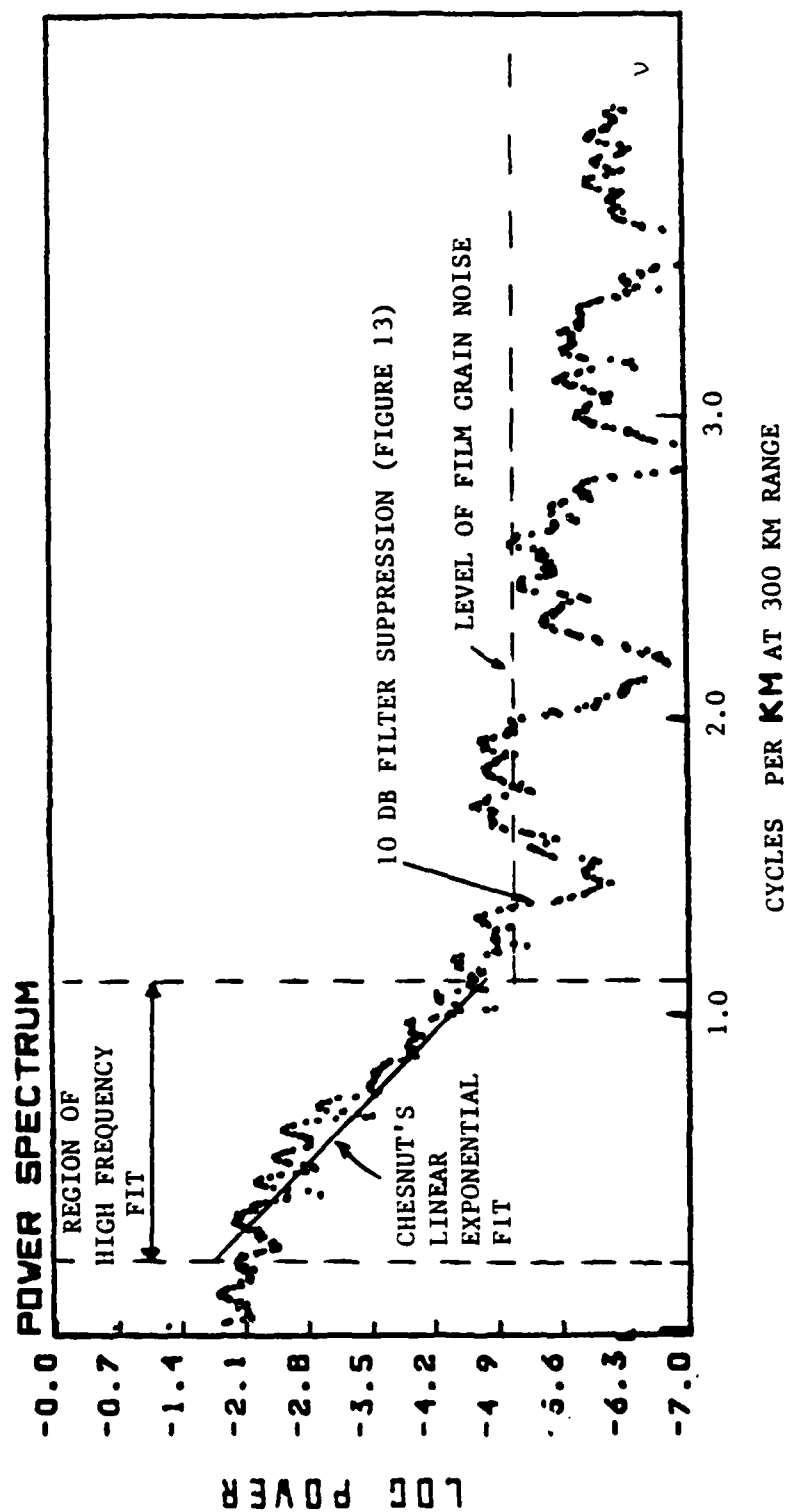


Figure 15- PSD resulting from profile of Figure 14 plotted on semi-log scale. Also shown (from Figure 13) are the region of high frequency fit, Chesnut's linear exponential fit, the film grain noise level, and the point of 10 db filter suppression.

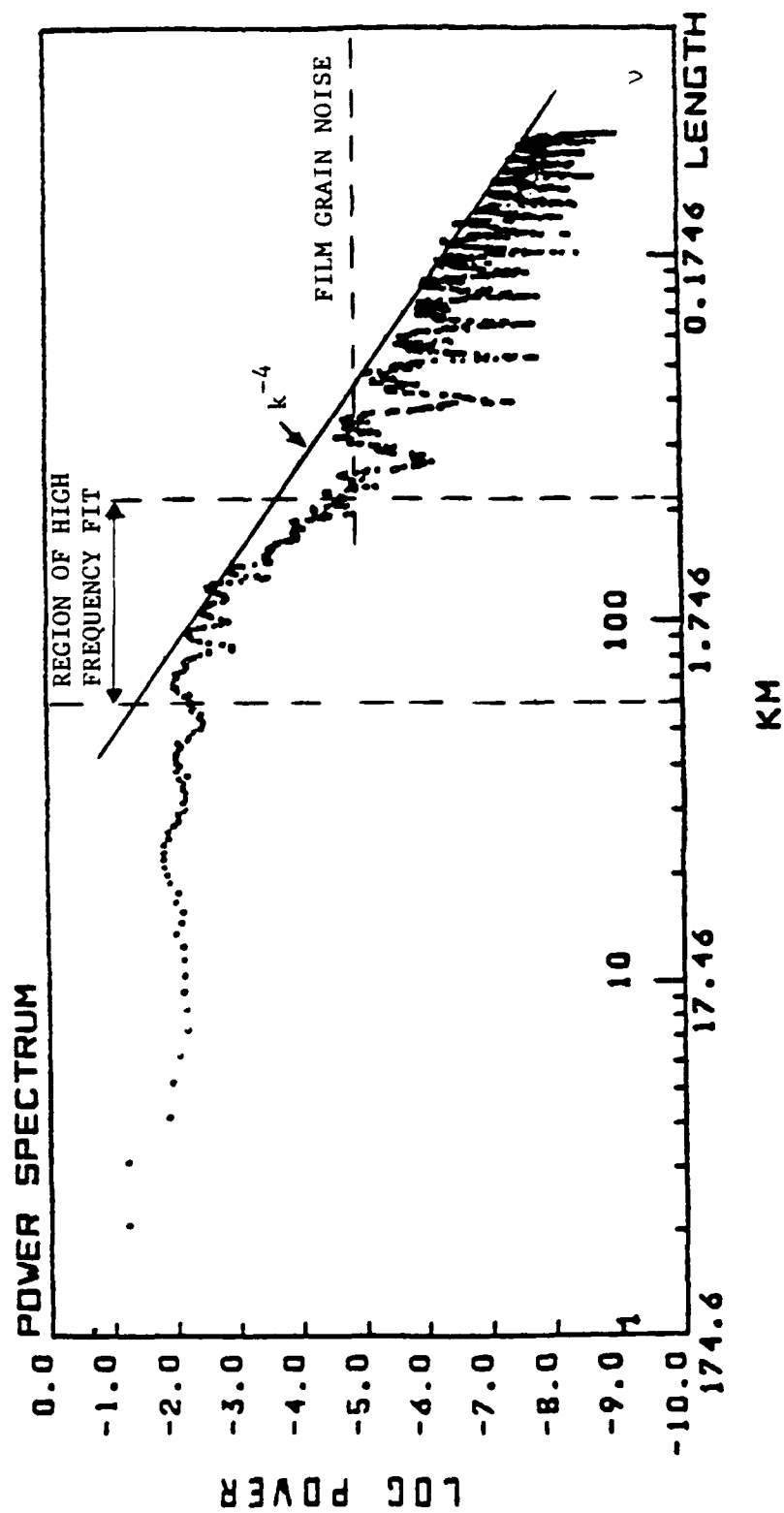


Figure 16- PSD of Figure 15 replotted on standard log-log plot.

REFERENCES

1. Mulbrandon, M., N.J. Zabusky, and E. Hyman, "Estimating Spectral Indices from Transforms of Discrete Representations of Density Functions, NRL Memorandum Report 5298, March 1984. (AD-A140 164)
2. Zabusky, N.J., E. Hyman, and M. Mulbrandon, "Projections of Plasma Cloud Structures and Their Spectra", NRL Memorandum Report 5561, March 1985.
3. Hyman, E., M. Mulbrandon, S.L. Ossakow, and B.E. McDonald, "Preliminary Numerical Simulation of IR Structure Development in a Hypothetical Uranium Release", NRL Memorandum Report 4659, November 1981. (AD-A107 600)
4. McDonald, B.E., M.J. Keskinen, S.L. Ossakow, and S.T. Zalesak, "Computer Simulation of Gradient Drift Instability Processes in Operation Avefria", J. Geophys. Res. 85, 2143 (1980). (AD-A077 668)
5. Zalesak, S.T., J.A. Fedder, and S.L. Ossakow, "Analysis and Numerical Simulation of the Effect of Ion Pedersen Mobility on Ionospheric Barium Clouds", J. Geophys. Res. 88, 8003 (1983).
6. Zalesak, S.T., P.K. Chaturvedi, S.L. Ossakow, and J.A. Fedder, "Finite Temperature Effects on the Evolution of Ionospheric Barium Clouds in the Presence of a Conducting Background Ionosphere I. A High Altitude Incompressible Background Ionosphere", NRL Memorandum Report 5346, July 1984 (AD-A143 592)

7. Chesnut, W.G., "Spatial-Frequency Analysis of Striated Nuclear Phenomena. Part Two: A Model of the Striated Check Mate Cloud," DNA 2757T-2, April 1972. (AD-522 611)

DISTRIBUTION LIST

DEPARTMENT OF DEFENSE

ASSISTANT SECRETARY OF DEFENSE
COMM, CMD, CONT 7 INTELL
WASHINGTON, D.C. 20301

DIRECTOR
COMMAND CONTROL TECHNICAL CENTER
PENTAGON RM BE 685
WASHINGTON, D.C. 20301
01CY ATTN C-650
01CY ATTN C-312 R. MASON

DIRECTOR
DEFENSE ADVANCED RSCH PROJ AGENCY
ARCHITECT BUILDING
1400 WILSON BLVD.
ARLINGTON, VA. 22209
01CY ATTN NUCLEAR
MONITORING RESEARCH
01CY ATTN STRATEGIC TECH OFFICE

DEFENSE COMMUNICATION ENGINEER CENTER
1860 WIEHLE AVENUE
RESTON, VA. 22090
01CY ATTN CODE R410
01CY ATTN CODE R812

DEFENSE TECHNICAL INFORMATION CENTER
CAMERON STATION
ALEXANDRIA, VA. 22314
02CY

DIRECTOR
DEFENSE NUCLEAR AGENCY
WASHINGTON, D.C. 20305
01CY ATTN STVL
04CY ATTN TITL
01CY ATTN DDST
03CY ATTN RAAE

COMMANDER
FIELD COMMAND
DEFENSE NUCLEAR AGENCY
KIRTLAND, AFB, NM 87115
01CY ATTN FCPR

DEFENSE NUCLEAR AGENCY
SAO/DNA
BUILDING 20676
KIRTLAND AFB, NM 87115
01CY D.C. THORNBURG

DIRECTOR
INTERSEVICE NUCLEAR WEAPONS SCHOOL
KIRTLAND AFB, NM 87115
01CY ATTN DOCUMENT CONTROL

JOINT CHIEFS OF STAFF
WASHINGTON, D.C. 20301
01CY ATTN J-3 WWMCCS EVALUATION
OFFICE

DIRECTOR
JOINT STRAT TGT PLANNING STAFF
OFFUTT AFB
OMAHA, NB 68113
01CY ATTN JSTPS/JLKS
01CY ATTN JPST G. GOETZ

CHIEF
LIVERMORE DIVISION FLD COMMAND DNA
DEPARTMENT OF DEFENSE
LAWRENCE LIVERMORE LABORATORY
P.O. BOX 808
LIVERMORE, CA 94550
01CY ATTN FCPRL

COMMANDANT
NATO SCHOOL (SHAPE)
APO NEW YORK 09172
01CY ATTN U.S. DOCUMENTS OFFICER

UNDER SECY OF DEF FOR RSCH & EMGRG
DEPARTMENT OF DEFENSE
WASHINGTON, D.C. 20301
01CY ATTN STRATEGIC & SPACE
SYSTEMS (OS)

WWMCCS SYSTEM ENGINEERING ORG
WASHINGTON, D.C. 20305
01CY ATTN R. CRAWFORD

COMMANDER/DIF CTOR
ATMOSPHERIC SCIENCES LABORATORY
U.S. ARMY ELECTRONICS COMMAND
WHITE SANDS MISSILE RANGE, NM 88002
O1CY ATTN DELAS-EO, F. NILES

DIRECTOR
BMD ADVANCED TECH CTR
HUNTSVILLE OFFICE
P.O. BOX 1500
HUNTSVILLE, AL 35807
O1CY ATTN ATC-T MELVIN T. CAPPS
O1CY ATTN ATC-O W. DAVIES
O1CY ATTN ATC-R DON RUSS

PROGRAM MANAGER
BMD PROGRAM OFFICE
5001 EISENHOWER AVENUE
ALEXANDRIA, VA 22333
O1CY ATTN DACS-BMT J. SHEA

CHIEF C-E- SERVICES DIVISION
U.S. ARMY COMMUNICATIONS CMD
PENTAGON RM 1B269
WASHINGTON, D.C. 20310
O1CY ATTN C- E-SERVICES DIVISION

COMMANDER
FRADCOM TECHNICAL SUPPORT ACTIVITY
DEPARTMENT OF THE ARMY
FORT MONMOUTH, N.J. 07703
O1CY ATTN DRSEL-NL-RD H. BENNET
O1CY ATTN DRSEL-PL-ENV H. BOMKE
O1CY ATTN J.E. QUIGLEY

COMMANDER
U.S. ARMY COMM-ELEC ENGRG INSTAL AGY
FT. HUACHUCA, AZ 85613
O1CY ATTN CCC-EMEO GEORGE LANE

COMMANDER
U.S. ARMY FOREIGN SCIENCE & TECH CTR
220 7TH STREET, NE
CHARLOTTESVILLE, VA 22901
O1CY ATTN DRXST-SD

COMMANDER
U.S. ARMY MATERIAL DEV & READINESS CMD
5001 EISENHOWER AVENUE
ALEXANDRIA, VA 22333
O1CY ATTN DRCLDC J.A. BENDER

COMMANDER
U.S. ARMY NUCLEAR AND CHEMICAL AGENCY
7500 BACKLICK ROAD
BLDG 2073
SPRINGFIELD, VA 22150
O1CY ATTN LIBRARY

DIRECTOR
U.S. ARMY BALLISTIC RESEARCH
LABORATORY
ABERDEEN PROVING GROUND, MD 21005
O1CY ATTN TECH LIBRARY,
EDWARD BAICY

COMMANDER
U.S. ARMY SATCOM AGENCY
FT. MONMOUTH, NJ 07703
O1CY ATTN DOCUMENT CONTROL

COMMANDER
U.S. ARMY MISSILE INTELLIGENCE AGENCY
REDSTONE ARSENAL, AL 35809
O1CY ATTN JIM GAMBLE

DIRECTOR
U.S. ARMY TRADOC SYSTEMS ANALYSIS
ACTIVITY
WHITE SANDS MISSILE RANGE, NM 88002
O1CY ATTN ATAA-SA
O1CY ATTN TCC/F. PAYAN JR.
O1CY ATTN ATTA-TAC LTC J. HESSE

COMMANDER
NAVAL ELECTRONIC SYSTEMS COMMAND
WASHINGTON, D.C. 20360
O1CY ATTN NAVALEX 034 T. HUGHES
O1CY ATTN PME 117
O1CY ATTN PME 117-T
O1CY ATTN CODE 5011

COMMANDING OFFICER
NAVAL INTELLIGENCE SUPPORT CTR
4301 SUITLAND ROAD, BLDG. 5
WASHINGTON, D.C. 20390
O1CY ATTN MR. DUBBIN STIC 12
O1CY ATTN NISC-50
O1CY ATTN CODE 5404 J. GALET

COMMANDER
NAVAL OCEAN SYSTEMS CENTER
SAN DIEGO, CA 92152
O1CY ATTN J. FERGUSON

NAVAL RESEARCH LABORATORY

WASHINGTON, D.C. 20375

01CY ATTN CODE 4700 S. L. Ossakow
26 CYS IF UNCLASS. 1 CY.
IF CLASS)
01CY ATTN CODE 4701 I Vitkovitsky
01CY ATTN CODE 4780 J. Huba (100
CYS IF UNCLASS, 1 CY IF CLASS)
01CY ATTN CODE 7500
01CY ATTN CODE 7550
01CY ATTN CODE 7580
01CY ATTN CODE 7551
01CY ATTN CODE 7555
01CY ATTN CODE 4730 E. MCLEAN
01CY ATTN CODE 4108
01CY ATTN CODE 4730 B. RIPIN
20CY ATTN CODE 2628

COMMANDER

NAVAL SPACE SURVEILLANCE SYSTEM

DAHLGREN, VA 22448

01CY ATTN CAPT J.H. BURTON

OFFICER-IN-CHARGE

NAVAL SURFACE WEAPONS CENTER

WHITE OAK, SILVER SPRING, MD 20910

01CY ATTN CODE F31

DIRECTOR

STRATEGIC SYSTEMS PROJECT OFFICE

DEPARTMENT OF THE NAVY

WASHINGTON, D.C. 20376

01CY ATTN NSP-2141

01CY ATTN NSSP-2722 FRED WIMBERLY

COMMANDER

NAVAL SURFACE WEAPONS CENTER

DAHLGREN LABORATORY

DAHLGREN, VA 22448

01CY ATTN CODE DF-14 R. BUTLER

OFFICER OF NAVAL RESEARCH

ARLINGTON, VA 22217

01CY ATTN CODE 465

01CY ATTN CODE 461

01CY ATTN CODE 402

01CY ATTN CODE 420

01CY ATTN CODE 421

COMMANDER

AEROSPACE DEFENSE COMMAND/DC

DEPARTMENT OF THE AIR FORCE

ENT AFB, CO 80912

01CY ATTN DC MR. LONG

COMMANDER

AEROSPACE DEFENSE COMMAND/XPD

DEPARTMENT OF THE AIR FORCE

ENT AFB, CO 80912

01CY ATTN XPDQQ

01CY ATTN XP

AIR FORCE GEOPHYSICS LABORATORY

HANSCOM AFB, MA 01731

01CY ATTN OPR HAROLD GARDNER

01CY ATTN LKB

KENNETH S.W. CHAMPION

01CY ATTN OPR ALVA T. STAIR

01CY ATTN PHD JURGEN RUCHAU

01CY ATTN PHD JOHN P. MULLEN

AF WEAPONS LABORATORY

KIRTLAND AFT, NM 87117

01CY ATTN SUL

01CY ATTN CA ARTHUR H. GUENTHER

01CY ATTN NTYCE 1LT. G. KRAJEI

AFTAC

PATRICK AFB, FL 32925

01CY ATTN TN

AIR FORCE AVIONICS LABORATORY

WRIGHT-PATTERSON AFB, OH 45433

01CY ATTN AAD WADE HUNT

01CY ATTN AAD ALLEN JOHNSON

DEPUTY CHIEF OF STAFF

RESEARCH, DEVELOPMENT, & ACQ

DEPARTMENT OF THE AIR FORCE

WASHINGTON, D.C. 20330

01CY ATTN AFRDQ

HEADQUARTERS

ELECTRONIC SYSTEMS DIVISION

DEPARTMENT OF THE AIR FORCE

HANSCOM AFB, MA 01731

01CY ATTN J. DEAS

HEADQUARTERS

ELECTRONIC SYSTEMS DIVISION/YSEA

DEPARTMENT OF THE AIR FORCE

HANSCOM AFB, MA 01732

01CY ATTN YSEA

HEADQUARTERS

ELECTRONIC SYSTEMS DIVISION/DC

DEPARTMENT OF THE AIR FORCE

HANSCOM AFB, MA 01731

01CY ATTN DCKC MAJ J.C. CLARK

COMMANDER
FOREIGN TECHNOLOGY DIVISION, AFSC
WRIGHT-PATTERSON AFB, OH 45433
01CY ATTN NICD LIBRARY
01CY ATTN ETD P B. BALLARD

COMMANDER
ROME AIR DEVELOPMENT CENTER, AFSC
GRIFFISS AFB, NY 13441
01CY ATTN DOC LIBRARY/TSLD
01CY ATTN OCSE V. COYNE

SAMSO/SZ
POST OFFICE BOX 92960
WORLDWAY POSTAL CENTER
LOS ANGELES, CA 90009
(SPACE DEFENSE SYSTEMS)
01CY ATTN SZJ

STRATEGIC AIR COMMAND/XPFS
OFFUTT AFB, NB 68113
01CY ATTN ADWATE MAJ BRUCE BAUER
01CY ATTN NRT
01CY ATTN DOK CHIEF SCIENTIST

SAMSO/SK
P.O. BOX 92960
WORLDWAY POSTAL CENTER
LOS ANGELES, CA 90009
01CY ATTN SKA (SPACE COMM SYSTEMS)
M. CLAVIN

SAMSO/MN
NORTON AFB, CA 92409
(MINUTEMAN)
01CY ATTN MNNL

COMMANDER
ROME AIR DEVELOPMENT CENTER, AFSC
HANSCOM AFB, MA 01731
01CY ATTN EEP A. LORENTZEN

DEPARTMENT OF ENERGY
LIBRARY ROOM G-042
WASHINGTON, D.C. 20545
01CY ATTN DOC CON FOR A. LABOWITZ

DEPARTMENT OF ENERGY
ALBUQUERQUE OPERATIONS OFFICE
P.O. BOX 5400
ALBUQUERQUE, NM 87115
01CY ATTN DOC CON FOR D. SHERWOOD

EG&G, INC.
LOS ALAMOS DIVISION
P.O. BOX 809
LOS ALAMOS, NM 85544
01CY ATTN DOC CON FOR J. BREEDLOVE

UNIVERSITY OF CALIFORNIA
LAWRENCE LIVERMORE LABORATORY
P.O. BOX 808
LIVERMORE, CA 94550
01CY ATTN DOC CON FOR TECH INFO
DEPT
01CY ATTN DOC CON FOR L-389 R. OTT
01CY ATTN DOC CON FOR L-31 R. HAGER

LOS ALAMOS NATIONAL LABORATORY
P.O. BOX 1663
LOS ALAMOS, NM 87545
01CY ATTN DOC CON FOR J. WOLCOTT
01CY ATTN DOC CON FOR R.F. TASCHEK
01CY ATTN DOC CON FOR E. JONES
01CY ATTN DOC CON FOR J. MALIK
01CY ATTN DOC CON FOR R. JEFFRIES
01CY ATTN DOC CON FOR J. ZINN
01CY ATTN DOC CON FOR P. KEATON
01CY ATTN DOC CON FOR D. WESTERVELT
01CY ATTN D. SAPPENFIELD

SANDIA LABORATORIES
P.O. BOX 5800
ALBUQUERQUE, NM 87115
01CY ATTN DOC CON FOR W. BROWN
01CY ATTN DOC CON FOR A.
THORNBROUGH
01CY ATTN DOC CON FOR T. WRIGHT
01CY ATTN DOC CON FOR D. DAHLGREN
01CY ATTN DOC CON FOR 3141
01CY ATTN DOC CON FOR SPACE PROJECT
DIV

SANDIA LABORATORIES
LIVERMORE LABORATORY
P.O. BOX 969
LIVERMORE, CA 94550
01CY ATTN DOC CON FOR B. MURPHEY
01CY ATTN DOC CON FOR T. COOK

OFFICE OF MILITARY APPLICATION
DEPARTMENT OF ENERGY
WASHINGTON, D.C. 20545
01CY ATTN DOC CON DR. YO SONG

OTHER GOVERNMENT

INSTITUTE FOR TELECOM SCIENCES
NATIONAL TELECOMMUNICATIONS & INFO
ADMIN
BOULDER, CO 80303

01CY ATTN A. JEAN (UNCLASS ONLY)
01CY ATTN W. UTLAUT
01CY ATTN D. CROMBIE
01CY ATTN L. BERRY

NATIONAL OCEANIC & ATMOSPHERIC ADMIN
ENVIRONMENTAL RESEARCH LABORATORIES
DEPARTMENT OF COMMERCE
BOULDER, CO 80302
01CY ATTN R. GRUBB
01CY ATTN AERONOMY LAB G. REID

DEPARTMENT OF DEFENSE CONTRACTORS

AEROSPACE CORPORATION
P.O. BOX 92957
LOS ANGELES, CA 90009
01CY ATTN I. GARFUNKEL
01CY ATTN T. SALMI
01CY ATTN V. JOSEPHSON
01CY ATTN S. BOWER
01CY ATTN D. OLSEN

ANALYTICAL SYSTEMS ENGINEERING CORP
5 OLD CONCORD ROAD
BURLINGTON, MA 01803
01CY ATTN RADIO SCIENCES

AUSTIN RESEARCH ASSOC., INC.
1901 RUTLAND DRIVE
AUSTIN, TX 78758
01CY ATTN L. SLOAN
01CY ATTN R. THOMPSON

BERKELEY RESEARCH ASSOCIATES, INC.
P.O. BOX 983
BERKELEY, CA 94701
01CY ATTN J. WORKMAN
01CY ATTN C. PRETTIE
01CY ATTN S. BRECHT

BOEING COMPANY, THE
P.O. BOX 3707
SEATTLE, WA 98124
01CY ATTN G. KEISTER
01CY ATTN D. MURRAY
01CY ATTN G. HALL
01CY ATTN J. KENNEY

CHARLES STARK DRAPER LABORATORY, INC.
555 TECHNOLOGY SQUARE
CAMBRIDGE, MA 02139
01CY ATTN D.B. COX
01CY ATTN J.P. GILMORE

COMSAT LABORATORIES
LINTHICUM ROAD
CLARKSBURG, MD 20734
01CY ATTN G. HYDE

CORNELL UNIVERSITY
DEPARTMENT OF ELECTRICAL ENGINEERING
ITHACA, NY 14850
01CY ATTN D.T. FARLEY, JR.

ELECTROSPACE SYSTEMS, INC.
BOX 1359
RICHARDSON, TX 75080
01CY ATTN H. LOGSTON
01CY ATTN SECURITY (PAUL PHILLIPS)

EOS TECHNOLOGIES, INC.
606 Wilshire Blvd.
Santa Monica, Calif 90401
01CY ATTN C.B. GARBARD
01CY ATTN R. LELEVIER

ESL, INC.
495 JAVA DRIVE
SUNNYVALE, CA 94086
01CY ATTN J. ROBERTS
01CY ATTN JAMES MARSHALL

GENERAL ELECTRIC COMPANY
SPACE DIVISION
VALLEY FORGE SPACE CENTER
GODDARD BLVD KING OF PRUSSIA
P.O. BOX 8555
PHILADELPHIA, PA 19101
01CY ATTN M.H. RORTNER
SPACE SCI LAB

GENERAL ELECTRIC COMPANY
P.O. BOX 1122
SYRACUSE, NY 13201
01CY ATTN F. REIBERT

GENERAL ELECTRIC TECH SERVICES
CO., INC.
HMES
COURT STREET
SYRACUSE, NY 13201
01CY ATTN G. MILLMAN

GEOPHYSICAL INSTITUTE
UNIVERSITY OF ALASKA
FAIRBANKS, AK 99701
(ALL CLASS ATTN: SECURITY OFFICER)
01CY ATTN T.N. DAVIS (UNCLASS ONLY)
01CY ATTN TECHNICAL LIBRARY
01CY ATTN NEAL BROWN (UNCLASS ONLY)

GTE SYLVANIA, INC.
ELECTRONICS SYSTEMS GRP-EASTERN DIV
77 A STREET
NEEDHAM, MA 02194
01CY ATTN DICK STEINHOF

HSS, INC.
2 ALFRED CIRCLE
BEDFORD, MA 01730
01CY ATTN DONALD HANSEN

ILLINOIS, UNIVERSITY OF
107 COBLE HALL
150 DAVENPORT HOUSE
CHAMPAIGN, IL 61820
(ALL CORRES ATTN DAN MCCLELLAND)
01CY ATTN K. YEH

INSTITUTE FOR DEFENSE ANALYSES
1801 NO. BEAUREGARD STREET
ALEXANDRIA, VA 22311
01CY ATTN J.M. AEIN
01CY ATTN ERNEST BAUER
01CY ATTN HANS WOLFARD
01CY ATTN JOEL BENGSTON

INTL TEL & TELEGRAPH CORPORATION
500 WASHINGTON AVENUE
NUTLEY, NJ 07110
01CY ATTN TECHNICAL LIBRARY

JAYCOR
11011 TORREYANA ROAD
P.O. BOX 85154
SAN DIEGO, CA 92138
01CY ATTN J.L. SPERLING

JOHNS HOPKINS UNIVERSITY
APPLIED PHYSICS LABORATORY
JOHNS HOPKINS ROAD
LAUREL, MD 20810
01CY ATTN DOCUMENT LIBRARIAN
01CY ATTN THOMAS POTEMRA
01CY ATTN JOHN DASSOULAS

KAMAN SCIENCES CORP
P.O. BOX 7463
COLORADO SPRINGS, CO 80933
01CY ATTN T. MEAGHER

KAMAN TEMPO-CENTER FOR ADVANCED
STUDIES
816 STATE STREET (P.O. DRAWER QQ)
SANTA BARBARA, CA 93102
01CY ATTN DASIAC
01CY ATTN WARREN S. KNAPP
01CY ATTN WILLIAM MCNAMARA
01CY ATTN B. GAMBILL

LINKABIT CORP
10453 ROSELLE
SAN DIEGO, CA 92121
01CY ATTN IRWIN JACOBS

LOCKHEED MISSILES & SPACE CO., INC
P.O. BOX 504
SUNNYVALE, CA 94088
01CY ATTN DEPT 60-12
01CY ATTN D.R. CHURCHILL

LOCKHEED MISSILES & SPACE CO., INC.
3251 HANOVER STREET
PALO ALTO, CA 94304
01CY ATTN MARTIN WALT DEPT 52-12
01CY ATTN W.L. IMHOF DEPT 52-12
01CY ATTN RICHARD G. JOHNSON
DEPT 52-12
01CY ATTN J.B. CLADIS DEPT 52-12

MARTIN MARIETTA CORP
ORLANDO DIVISION
P.O. BOX 5837
ORLANDO, FL 32805
01CY ATTN R. HEFFNER

M.I.T. LINCOLN LABORATORY
P.O. BOX 73
LEXINGTON, MA 02173
01CY ATTN DAVID M. TOWLE
01CY ATTN L. LOUGHLIN
01CY ATTN D. CLARK

MCDONNELL DOUGLAS CORPORATION
5301 BOLSA AVENUE
HUNTINGTON BEACH, CA 92647

01CY ATTN N. HARRIS
01CY ATTN J. MOULE
01CY ATTN GEORGE MROZ
01CY ATTN W. OLSON
01CY ATTN R.W. HALPRIN
01CY ATTN TECHNICAL
LIBRARY SERVICES

MISSION RESEARCH CORPORATION
735 STATE STREET

SANTA BARBARA, CA 93101
01CY ATTN P. FISCHER
01CY ATTN W.F. CREVIER
01CY ATTN STEVEN L. GUTSCHE
01CY ATTN R. BOGUSCH
01CY ATTN R. HENDRICK
01CY ATTN RALPH KILB
01CY ATTN DAVE SOWLE
01CY ATTN F. FAJEN
01CY ATTN M. SCHEIBE
01CY ATTN CONRAD L. LONGMIRE
01CY ATTN B. WHITE
01CY ATTN R. STAGAT

MISSION RESEARCH CORP.
1720 RANDOLPH ROAD, S.E.
ALBUQUERQUE, NEW MEXICO 87106
01CY R. STELLINGWERF
01CY M. ALME
01CY L. WRIGHT

MITRE CORPORATION, THE
P.O. BOX 208
BEDFORD, MA 01730
01CY ATTN JOHN MORGANSTERN
01CY ATTN G. HARDING
01CY ATTN C.E. CALLAHAN

MITRE CORP
WESTGATE RESEARCH PARK
1820 DOLLY MADISON BLVD
MCLEAN, VA 22101
01CY ATTN W. HALL
01CY ATTN W. FOSTER

PACIFIC-SIERRA RESEARCH CORP
12340 SANTA MONICA BLVD.
LOS ANGELES, CA 90025
01CY ATTN E.C. FIELD, JR.

PENNSYLVANIA STATE UNIVERSITY
IONOSPHERE RESEARCH LAB
318 ELECTRICAL ENGINEERING EAST
UNIVERSITY PARK, PA 16802
(NO CLASS TO THIS ADDRESS)
01CY ATTN IONOSPHERIC RESEARCH LAB

PHOTOMETRICS, INC.
4 ARROW DRIVE
WOBBURN, MA 01801
01CY ATTN IRVING L. KOFSKY

PHYSICAL DYNAMICS, INC.
P.O. BOX 3027
BELLEVUE, WA 98009
01CY ATTN E.J. FREMOUW

PHYSICAL DYNAMICS, INC.
P.O. BOX 10367
OAKLAND, CA 94610
ATTN A. THOMSON

R & D ASSOCIATES
P.O. BOX 9695
MARINA DEL REY, CA 90291
01CY ATTN FORREST GILMORE
01CY ATTN WILLIAM B. WRIGHT, JR.
01CY ATTN WILLIAM J. KARZAS
01CY ATTN H. ORY
01CY ATTN C. MACDONALD
01CY ATTN R. TURCO
01CY ATTN L. DeRAND
01CY ATTN W. TSAI

RAND CORPORATION, THE
1700 MAIN STREET
SANTA MONICA, CA 90406
01CY ATTN CULLEN CRAIN
01CY ATTN ED REDROZIAN

RAYTHEON CO.
528 BOSTON POST ROAD
SUDBURY, MA 01776
01CY ATTN BARBARA ADAMS

RIVERSIDE RESEARCH INSTITUTE
330 WEST 42nd STREET
NEW YORK, NY 10036
01CY ATTN VINCE TRAPANI

SCIENCE APPLICATIONS, INC.

1150 PROSPECT PLAZA

LA JOLLA, CA 92037

01CY ATTN LEWIS M. LINSON

01CY ATTN DANIEL A. HAMLIN

01CY ATTN E. FRIEMAN

01CY ATTN E.A. STRAKER

01CY ATTN CURTIS A. SMITH

SCIENCE APPLICATIONS, INC

1710 GOODRIDGE DR.

MCLEAN, VA 22102

01CY J. COCKAYNE

01CY E. HYMAN

SRI INTERNATIONAL

333 RAVENSWOOD AVENUE

MENLO PARK, CA 94025

01CY ATTN J. CASPER

01CY ATTN DONALD NEILSON

01CY ATTN ALAN BURNS

01CY ATTN G. SMITH

01CY ATTN R. TSUNODA

01CY ATTN DAVID A. JOHNSON

01CY ATTN WALTER G. CHESNUT

01CY ATTN CHARLES L. RINO

01CY ATTN WALTER JAYE

01CY ATTN J. VICKREY

01CY ATTN RAY L. LEADABRAND

01CY ATTN G. CARPENTER

01CY ATTN G. PRICE

01CY ATTN R. LIVINGSTON

01CY ATTN V. GONZALES

01CY ATTN D. MCDANIEL

TECHNOLOGY INTERNATIONAL CORP

75 WIGGINS AVENUE

BEDFORD, MA 01730

01CY ATTN W.P. BOQUIST

TOYON RESEARCH CO.

P.O. Box 6890

SANTA BARBARA, CA 93111

01CY ATTN JOHN ISE, JR.

01CY ATTN JOEL GARBARINO

TRW DEFENSE & SPACE SYS GROUP

ONE SPACE PARK

REDONDO BEACH, CA 90278

01CY ATTN R. K. PLEBUCH

01CY ATTN S. ALTSCHULER

01CY ATTN D. DEE

01CY ATTN D/ STOCKWELL

SNTF/1575

VISIDYNE

SOUTH BEDFORD STREET

BURLINGTON, MASS 01803

01CY ATTN W. REIDY

01CY ATTN J. CARPENTER

01CY ATTN C. HUMPHREY

UNIVERSITY OF PITTSBURGH

PITTSBURGH, PA 15213

01CY ATTN: N. ZABUSKY

DIRECTOR OF RESEARCH

U.S. NAVAL ACADEMY

ANNAPOLIS, MD 21402

02CY

END

DT/C

8-86